

Double field inflation of generalized dilaton-axion models with a new Fayet-Iliopoulos (FI) term

MAN Ping Kwan, Ellgan^{a)†}

Department of Pure and Applied Physics, Waseda University^{a)}

1 Abstract

We study the inflation dynamics of generalized dilaton-axion models with a new Fayet-Iliopoulos (FI) term. In particular, we find the relationships between the super-potential parameters and the coefficient of natural logarithm of the real part of dilaton-axion fields stored in the Kähler potential based on the vacuum conditions at the end of inflation. We also evaluate the feasible initial field values, their corresponding SUSY breaking scales and the iso-curvature parameters.

2 Introduction

Slow-roll parameters	Range(s)	Spectral indices	Range(s)
ϵ_V	< 0.004	$n_s - 1$	$[-0.0423, -0.0327]$
η_V	$[-0.021, -0.008]$	$\frac{dn_s}{d\ln k}$	$[-0.008, 0.012]$
ξ_V	$[-0.0045, 0.0096]$	$\frac{d^2 n_s}{d\ln k^2}$	$[-0.003, 0.023]$
H_{hc}	$< 2.7 \times 10^{-5} M_{\text{pl}}$	V_{hc}	$< (1.7 \times 10^{16} \text{ GeV})^4$

Table 1: Slow roll potential parameters and spectral indices in Planck 2018

Inflation is the vital part for studying the birth of our universe and verifying the consistency of the theory of quantum gravity [1, 2, 3]. The latest observation data are shown in Table 1 [5], which are consistent with the slow roll approximation. There are many models satisfying the observation [4, 5], one of which is the most promising model - Starobinsky model (also called R^2 inflation model), which can be motivated by, for example, modified gravity theory [2, 4, 10, 11, 12, 13, 14] and supergravity theory (SUGRA) [15, 16, 17, 18]. Since SUGRA describes high energy physics beyond the Standard model (SM), gravity beyond the Λ CDM cosmological model and the low energy effective theory of superstring theory, it has been adopted to study the primordial dynamics of the universe evolution. In particular, the extension of Starobinsky model in the new-minimal formulation of SUGRA is dual to the standard counterpart coupled to a massive vector multiplet, or a massless vector multiplet and a Stückelberg chiral multiplet with the Kähler potential in the following form [19, 20, 21]

$$\frac{K(T, \bar{T})}{M_{\text{pl}}^2} = -\rho \ln \left(\frac{T + \bar{T}}{M_{\text{pl}}} \right) + \tilde{\beta} \left(\frac{T + \bar{T}}{M_{\text{pl}}} \right), \quad (1)$$

where the last term is the FI term of the gauged R -symmetry and spontaneous SUSY breaking occurred after the inflation. [21] showed that this model can be consistent with observations

^{a)}MAN Ping Kwan, Ellgan, E-mail: ellgan101@akane.waseda.jp

only for $\rho = 1, 2$ with some non-perturbative corrections and SUSY is spontaneously broken at the dS vacuum with gravitino mass in the TeV range. Furthermore, [24] finds that an alternative non-vanishing FI terms [22, 23] can allow inflationary models having the following forms of Kähler potential K

$$\frac{K(T, \bar{T})}{M_{\text{pl}}^2} = -\rho \ln \left(\frac{T + \bar{T}}{M_{\text{pl}}} \right). \quad (2)$$

This Kähler potential model generalizes various models such as no-scale SUGRA [25, 26, 27, 28, 29, 30, 31] and M theory compactification on a G_2 manifold [32, 33, 34]. The model studied in [24] describes the inflation from the real part of dilaton-axion chiral superfield T with a fixed imaginary part at the dS vacuum. Thus, it is interesting to see how the inflation dynamics changes when the imaginary part also evolves to contribute to the inflation dynamics. That is the main theme of this paper.

In this paper, we are going to study the inflation dynamics of generalized dilaton-axion models, where both the dilaton and its axionic partner simultaneously contribute to the evolution of inflation. The organization of this paper is as follows. In section 3, we give the total potential consisting of F term from the Kähler potential given by Eq.(2) and the Polonyi type superpotential, and D term potential from an alternative FI term [22, 23]. We give the derivatives of the total potential, the possible ranges of parameters under the constraints of dS vacuum and the corresponding SUSY breaking scales in section 4. We summarize our results of dS vacuum in section 5 and the equations of motion (E.O.M.s) of the evolution of dilaton and axion. In section 6, we give the initial conditions and parameters feasible for inflation based on the constraints of Planck observation listed in Table 1 and e-folding number 50 to 60. We discuss our results in section 7 and draw conclusions in section 8.

3 General model

Recall the F term potential in $\mathcal{N} = 1$ supergravity (SUGRA) is

$$V_F = e^{\frac{K}{M_{\text{pl}}^2}} \left(K^{I\bar{J}} D_I W D_{\bar{J}} \bar{W} - \frac{3}{M_{\text{pl}}^2} |W|^2 \right). \quad (3)$$

where

$$K_{I\bar{J}} \equiv \frac{\partial^2 K}{\partial \Phi^I \partial \bar{\Phi}^{\bar{J}}}, \quad D_I W \equiv \partial_I W + \frac{1}{M_{\text{pl}}^2} (\partial_I K) W = \frac{\partial W}{\partial \Phi^I} + \frac{1}{M_{\text{pl}}^2} \frac{\partial K}{\partial \Phi^I} W, \quad (4)$$

Φ^I is complex scalar field for all I from 1 to the dimension of the field space, the upper bar means the complex conjugate of the corresponding variables/ fields, $K^{I\bar{J}}$ is the inverse of the Kähler metric $K_{I\bar{J}}$ and M_{pl} is the (reduced) Planck mass¹. Note that the Kähler potential is given by

$$\frac{K(T, \bar{T})}{M_{\text{pl}}^2} = -\rho \ln \left(\frac{T + \bar{T}}{M_{\text{pl}}} \right), \quad (5)$$

while the super-potential is given by

$$W(T) = \lambda + \mu T, \quad (6)$$

¹Since the mass dimensions of Kähler potential K and super-potential W are 2 and 3 respectively, the (F term) potential V_F has the mass dimension of 4. (i.e. $[K] = M_{\text{pl}}^2$, $[W] = M_{\text{pl}}^3$, $[V_F] = M_{\text{pl}}^4$)

where $\rho \in \mathbb{N}$ and $\lambda, \mu \in \mathbb{C}$ are constants². Note that the first and second derivatives of the Kähler potential are given by

$$K_T = K_{\bar{T}} = \frac{-\rho M_{\text{pl}}^2}{T + \bar{T}}, \quad K_{T\bar{T}} = \frac{\rho M_{\text{pl}}^2}{(T + \bar{T})^2}, \quad (7)$$

The first covariant (Kähler) derivative of potential is

$$D_T W = \mu - \frac{\rho}{T + \bar{T}} (\lambda + \mu T), \quad (8)$$

and the F term potential is

$$V_F = \frac{-1}{M_{\text{pl}}^2} \left(\frac{\bar{T} + T}{M_{\text{pl}}} \right)^{-\rho} \left\{ \bar{\lambda} (\mu \bar{T} + 2\lambda + 3\mu T) + \bar{\mu} (\bar{T}(3\lambda + 2\mu T) + \lambda T) \right\}, \quad (9)$$

or in terms of $\lambda = \lambda_R + i\lambda_I$, $\mu = \mu_R + i\mu_I$, $T = T_R + iT_I$, $\omega_1 = 2(\lambda_R \mu_R + \lambda_I \mu_I)$, $\omega_2 = 2(\lambda_I \mu_R - \lambda_R \mu_I)$, $\omega_1^2 + \omega_2^2 = 4|\mu|^2 |\lambda|^2$, $\omega_1 = \iota_1 |\mu|^2$, $\omega_2 = \iota_2 |\mu|^2$,

$$M_{\text{pl}}^2 V_F = \left(\frac{M_{\text{pl}}}{2T_R} \right)^\rho \left\{ (\rho - 3) (|\lambda|^2 + \omega_2 T_I + |\mu|^2 T_I^2) + (\rho - 5) \omega_1 T_R + \frac{(\rho^2 - 7\rho + 4)}{\rho} |\mu|^2 T_R^2 \right\}. \quad (10)$$

For simplicity, we let

$$A(T_I) = \frac{1}{M_{\text{pl}}^2} \left(\frac{M_{\text{pl}}}{2} \right)^\rho (\rho - 3) (|\lambda|^2 + \omega_2 T_I + |\mu|^2 T_I^2), \quad (11)$$

$$B = \frac{1}{M_{\text{pl}}^2} \left(\frac{M_{\text{pl}}}{2} \right)^\rho (\rho - 5) \omega_1, \quad C = \frac{1}{M_{\text{pl}}^2} \left(\frac{M_{\text{pl}}}{2} \right)^\rho \frac{(\rho^2 - 7\rho + 4)}{\rho} |\mu|^2, \quad (12)$$

so that the F term potential becomes

$$V_F = A(T_I) T_R^{-\rho} + B T_R^{1-\rho} + C T_R^{2-\rho}. \quad (13)$$

Even though the vacuum of a F term potential is generally AdS, we can obtain the dS vacuum by introducing an abelian vector multiplet with the simplest Fayet-Iliopoulos (FI) type term [22, 23] and eliminating the auxiliary field of the vector multiplet, which has a positive contribution [24]

$$V_D = \frac{1}{2} g^2 \xi^2, \quad (14)$$

where g is the gauge coupling and ξ is the real FI constant. Hence, in the rest of this paper, we investigate the properties and inflation dynamics of the total potential $V = V_F + V_D$.

4 Derivatives of the total potential

To find our present universe after inflation, we set up some constraints on the derivatives of the F term potential to find the minimum as follows. The first derivatives are

$$\frac{\partial V}{\partial T_R} = -\rho A(T_I) T_R^{-\rho-1} + (1 - \rho) B T_R^{-\rho} + (2 - \rho) C T_R^{1-\rho}, \quad (15)$$

²The mass dimensions of ρ , λ , λ_R , λ_I , μ , μ_R , μ_I , T , T_R and T_I are $[\rho] = 1$, $[\lambda] = [\lambda_R] = [\lambda_I] = M_{\text{pl}}^3$, $[\mu] = [\mu_R] = [\mu_I] = M_{\text{pl}}^2$, $[T] = [T_R] = [T_I] = M_{\text{pl}}$.

$$\frac{\partial V}{\partial T_I} = \frac{1}{M_{\text{pl}}^2} \left(\frac{M_{\text{pl}}}{2T_R} \right)^\rho (\rho - 3) (\omega_2 + 2|\mu|^2 T_I), \quad (16)$$

while the second derivatives are

$$\frac{\partial^2 V}{\partial T_R^2} = (\rho + 1) \rho A(T_I) T_R^{-\rho-2} + \rho(\rho - 1) B T_R^{-\rho-1} + (\rho - 1)(\rho - 2) C T_R^{-\rho}, \quad (17)$$

$$\frac{\partial^2 V}{\partial T_R \partial T_I} = \frac{\partial^2 V}{\partial T_I \partial T_R} = \frac{-2}{M_{\text{pl}}^3} \left(\frac{M_{\text{pl}}}{2T_R} \right)^{\rho+1} (\rho - 3) \rho (\omega_2 + 2|\mu|^2 T_I), \quad (18)$$

$$\frac{\partial^2 V}{\partial T_I^2} = \frac{2}{M_{\text{pl}}^2} \left(\frac{M_{\text{pl}}}{2T_R} \right)^\rho (\rho - 3) |\mu|^2. \quad (19)$$

The minimum points are the solutions of the following equations

$$\begin{aligned} \frac{\partial V}{\partial T_R} &= -T_R^{-\rho-1} \{ \rho A(T_I) + (\rho - 1) B T_R + (\rho - 2) C T_R^2 \} = 0 \\ \Rightarrow T_R &= \frac{-(\rho - 1) B \pm \sqrt{(\rho - 1)^2 B^2 - 4\rho(\rho - 2) A(T_I) C}}{2(\rho - 2) C}, \end{aligned} \quad (20)$$

$$\frac{\partial V}{\partial T_I} = \frac{1}{M_{\text{pl}}^2} \left(\frac{M_{\text{pl}}}{2T_R} \right)^\rho (\rho - 3) (\omega_2 + 2|\mu|^2 T_I) = 0 \quad \Rightarrow \quad T_I = \frac{-\omega_2}{2|\mu|^2} = -\frac{\iota_2}{2} \quad \text{or} \quad \rho = 3, \quad (21)$$

4.1 Suppose $\rho \neq 3$.

When $T_I = \frac{-\omega_2}{2|\mu|^2} = T_{I0}$, we have

$$A(T_{I0}) = \frac{\rho - 3}{M_{\text{pl}}^2} \left(\frac{M_{\text{pl}}}{2} \right)^\rho \left(|\lambda|^2 - \frac{\omega_2^2}{4|\mu|^2} \right) = \frac{\rho - 3}{M_{\text{pl}}^2} \left(\frac{M_{\text{pl}}}{2} \right)^\rho \frac{\omega_1^2}{4|\mu|^2}, \quad (22)$$

and B and C are given by Eq.(12). The critical values of T_R are given by

$$T_{R0} = \frac{\rho [-(\rho - 1)(\rho - 5) \pm (\rho + 1)] \omega_1}{2(\rho - 2)(\rho^2 - 7\rho + 4) |\mu|^2} = \frac{-\rho(\rho - 3)}{2(\rho^2 - 7\rho + 4)} \frac{\omega_1}{|\mu|^2} \quad \text{or} \quad \frac{-\rho}{2(\rho - 2)} \frac{\omega_1}{|\mu|^2}. \quad (23)$$

Defining

$$T_{R0-} = \frac{-\rho(\rho - 3) \iota_1}{2(\rho^2 - 7\rho + 4)} \quad \text{and} \quad T_{R0+} = \frac{-\rho \iota_1}{2(\rho - 2)}, \quad (24)$$

we know that the positivity of T_{R0} give the ranges³ of ρ as shown in Table 2.

To check whether the potential is physical at the critical points⁴, the mass matrix evaluated at (T_{R0-}, T_{I0}) is

$$\left(\begin{array}{cc} \frac{\partial^2 V}{\partial T_R^2} & \frac{\partial^2 V}{\partial T_R \partial T_I} \\ \frac{\partial^2 V}{\partial T_I \partial T_R} & \frac{\partial^2 V}{\partial T_I^2} \end{array} \right) \bigg|_{(T_{R0-}, T_{I0})} = \frac{2|\mu|^2}{M_{\text{pl}}^2} \left[\frac{(\rho^2 - 7\rho + 4) M_{\text{pl}}}{-\rho(\rho - 3) \iota_1} \right]^\rho \left(\begin{array}{cc} \frac{-(\rho+1)(\rho^2-7\rho+4)}{\rho(\rho-3)} & 0 \\ 0 & (\rho - 3) \end{array} \right), \quad (25)$$

³Note that the roots of $\rho^2 - 7\rho + 4 = 0$ are $\rho = \frac{1}{2}(7 - \sqrt{33}) \approx 0.627719$ or $\rho = \frac{1}{2}(7 + \sqrt{33}) \approx 6.37228$.

⁴It means the eigenvalues of the mass matrix are all positive.

Case(s)	$T_{R0-} > 0$	$T_{R0+} > 0$
$\omega_1 > 0$ ($\iota_1 > 0$)	$0 < \rho < \frac{(7-\sqrt{33})}{2}, 3 < \rho < \frac{(7+\sqrt{33})}{2}$	$0 < \rho < 2$
$\omega_1 < 0$ ($\iota_1 < 0$)	$\rho < 0, \frac{(7-\sqrt{33})}{2} < \rho < 3, \rho > \frac{(7+\sqrt{33})}{2}$	$\rho < 0, \rho > 2$

Table 2: Possible ranges for satisfying the positivity of T_{R0}

which has two positive eigenvalues if $3 < \rho < \frac{7+\sqrt{33}}{2}$. The corresponding square masses of T_R and T_I (evaluated at (T_{R0-}, T_{I0})) are

$$M_{T_R}^2|_{(T_{R0-}, T_{I0})} = \frac{2|\mu|^2}{M_{\text{pl}}^2} \left[\frac{(\rho^2 - 7\rho + 4) M_{\text{pl}}}{-\rho(\rho - 3)\iota_1} \right]^\rho \frac{(\rho + 1)(\rho^2 - 7\rho + 4)}{-\rho(\rho - 3)}, \quad (26)$$

$$M_{T_I}^2|_{(T_{R0-}, T_{I0})} = \frac{2|\mu|^2}{M_{\text{pl}}^2} \left[\frac{(\rho^2 - 7\rho + 4) M_{\text{pl}}}{-\rho(\rho - 3)\iota_1} \right]^\rho (\rho - 3), \quad (27)$$

while their ratio is

$$\left(\frac{M_{T_R}}{M_{T_I}} \right)^2 \Big|_{(T_{R0-}, T_{I0})} = \frac{(\rho + 1)(\rho^2 - 7\rho + 4)}{-\rho(\rho - 3)^2}. \quad (28)$$

The counterpart evaluated (T_{R0+}, T_{I0})

$$\left(\begin{array}{cc} \frac{\partial^2 V}{\partial T_R^2} & \frac{\partial^2 V}{\partial T_R \partial T_I} \\ \frac{\partial^2 V}{\partial T_I \partial T_R} & \frac{\partial^2 V}{\partial T_I^2} \end{array} \right) \Big|_{(T_{R0+}, T_{I0})} = \frac{2|\mu|^2}{M_{\text{pl}}^2} \left[\frac{(\rho - 2) M_{\text{pl}}}{-\rho\iota_1} \right]^\rho \left(\begin{array}{cc} \frac{(\rho+1)(\rho-2)}{\rho} & 0 \\ 0 & (\rho - 3) \end{array} \right). \quad (29)$$

which has two positive eigenvalues if $\rho > 3$ and the corresponding square masses of T_R and T_I (evaluated at (T_{R0+}, T_{I0})) are

$$M_{T_R}^2|_{(T_{R0+}, T_{I0})} = \frac{2|\mu|^2}{M_{\text{pl}}^2} \left[\frac{(\rho - 2) M_{\text{pl}}}{-\rho\iota_1} \right]^\rho \frac{(\rho + 1)(\rho - 2)}{\rho}, \quad (30)$$

$$M_{T_I}^2|_{(T_{R0+}, T_{I0})} = \frac{2|\mu|^2}{M_{\text{pl}}^2} \left[\frac{(\rho - 2) M_{\text{pl}}}{-\rho\iota_1} \right]^\rho (\rho - 3), \quad (31)$$

while their ratio is

$$\left(\frac{M_{T_R}}{M_{T_I}} \right)^2 \Big|_{(T_{R0+}, T_{I0})} = \frac{(\rho + 1)(\rho - 2)}{\rho(\rho - 3)}. \quad (32)$$

Combining with the ranges given by the positivity of T_{R0} , we can finalize the possible ranges to produce a dS vacuum as shown in Table 3. Now, based on the physically feasible ranges,

Case(s)	$T_{R0-} > 0, \lambda_{1,2} > 0$	$T_{R0+} > 0, \lambda_{1,2} > 0$
$\omega_1 > 0$ ($\iota_1 > 0$)	$3 < \rho < \frac{7+\sqrt{33}}{2}$	\times
$\omega_1 < 0$ ($\iota_1 < 0$)	\times	$\rho > 3$

Table 3: Possible ranges for satisfying the positivity of T_{R0} and positive eigenvalues of the mass matrix λ_1, λ_2

we can obtain the corresponding gravitino mass and the F term and D term SUSY breaking scales.

4.1.1 Suppose $\omega_1 > 0$, $3 < \rho < \frac{7+\sqrt{33}}{2}$.

The gravitino mass evaluated at (T_{R0-}, T_{I0}) is

$$M_{3/2-} \equiv \frac{e^{\frac{K}{2M_{\text{pl}}^2}}}{M_{\text{pl}}^2} |W(T)| \Big|_- = \frac{1}{M_{\text{pl}}^2} \left(\frac{M_{\text{pl}}(\rho-2)(\rho^2-7\rho+4)}{-(\rho-3)\rho\iota_1} \right)^{\rho/2} \times \left| \frac{(\rho^3-10\rho^2+21\rho-8)\iota_1\mu}{2(\rho-2)(\rho^2-7\rho+4)} \right|, \quad (33)$$

which forms the following ratios with

$$\left(\frac{M_{T_R}}{M_{3/2}} \right)^2 \Big|_{(T_{R0-}, T_{I0})} = \frac{-8(\rho+1)(\rho^2-7\rho+4)^3}{(\rho-2)^{(\rho-2)}\rho(\rho-3)(\rho^3-10\rho^2+21\rho-8)^2} \left(\frac{M_{\text{pl}}}{\iota_1} \right)^2, \quad (34)$$

The F term SUSY breaking scale evaluated at (T_{R0-}, T_{I0}) is

$$F_T|_- \equiv e^{\frac{K}{2M_{\text{pl}}^2}} |D_T W(T)| \Big|_- = \left(\frac{M_{\text{pl}}(\rho-2)(\rho^2-7\rho+4)}{-(\rho-3)\rho\iota_1} \right)^{\rho/2} \times \left| \frac{(\rho-7)(\rho-2)(\rho-1)\mu}{2(\rho-3)} \right|. \quad (35)$$

while the D term SUSY breaking scale evaluated at (T_{R0-}, T_{I0}) is

$$\frac{1}{2}g^2\xi^2 \Big|_- \equiv \frac{\iota_1|\mu|^2}{\rho M_{\text{pl}}} \left(\frac{(\rho^2-7\rho+4)M_{\text{pl}}}{-(\rho-3)\rho\iota_1} \right)^{\rho-1}. \quad (36)$$

4.1.2 Suppose $\omega_1 < 0$, $\rho > 3$.

The gravitino mass evaluated at (T_{R0+}, T_{I0}) is

$$M_{3/2+} \equiv \frac{e^{\frac{K}{2M_{\text{pl}}^2}}}{M_{\text{pl}}^2} |W(T)| \Big|_+ = \frac{1}{M_{\text{pl}}^2} \left(\frac{(\rho-2)M_{\text{pl}}}{-\rho\iota_1} \right)^{\rho/2} \times \left| \frac{-\iota_1\mu}{(\rho-2)} \right|, \quad (37)$$

and the F term SUSY breaking scale evaluated at (T_{R0+}, T_{I0}) is

$$F_T|_+ \equiv e^{\frac{K}{2M_{\text{pl}}^2}} |D_T W(T)| \Big|_+ = \left(\frac{(\rho-2)M_{\text{pl}}}{-\rho\iota_1} \right)^{\rho/2} \times |0| = 0. \quad (38)$$

while the D term SUSY breaking scale evaluated at (T_{R0+}, T_{I0}) is

$$\frac{1}{2}g^2\xi^2 \Big|_+ \equiv \frac{3\iota_1^2|\mu|^2}{M_{\text{pl}}^2(\rho-2)^2} \left(\frac{(\rho-2)M_{\text{pl}}}{-\rho\iota_1} \right)^\rho. \quad (39)$$

4.2 Suppose $\rho = 3$.

The total potential becomes

$$V = -\frac{M_{\text{pl}}}{3(\bar{T}+T)^2} [3\mu\bar{\lambda} + \bar{\mu}(2\mu\bar{T} + 3\lambda + 2\mu T)] + \frac{1}{2}g^2\xi^2, \quad (40)$$

or in terms of $\lambda = \lambda_R + i\lambda_I$, $\mu = \mu_R + i\mu_I$, $T = T_R + iT_I$, $\omega_1 = 2(\lambda_R\mu_R + \lambda_I\mu_I)$, $\omega_2 = 2(\lambda_I\mu_R - \lambda_R\mu_I)$,

$$V(T_R) = \frac{-M_{\text{pl}}}{8T_R^3} \left(\frac{8}{3} |\mu|^2 T_R^2 + 2T_R\omega_1 \right) + \frac{1}{2} g^2 \xi^2, \quad (41)$$

which is independent of the imaginary part of T , T_I . This model does not form a double field inflation model since the second derivative of V with respect to T_I , $\frac{\partial^2 V}{\partial T_I^2}$ is equal to zero, but it can be considered as a single field model if we fix T_I to some real values. To consider it as a single field model and study the properties of minimum point, we first find the first and second derivatives

$$\frac{\partial V}{\partial T_R} = \frac{M_{\text{pl}}}{6T_R^3} (2|\mu|^2 T_R + 3\omega_1) \quad (42)$$

$$\frac{\partial^2 V}{\partial T_R^2} = \frac{-M_{\text{pl}}}{6T_R^4} (4|\mu|^2 T_R + 9\omega_1) \quad (43)$$

Finding the minimum point by taking $\frac{\partial V}{\partial T_R} = 0$, we have

$$\frac{\partial V}{\partial T_R} = 0 \quad \Rightarrow \quad T_R = \frac{-3\omega_1}{2|\mu|^2} = \frac{-3\iota_1}{2} =: T_{R0}. \quad (44)$$

The second derivative evaluated at $T_R = T_{R0}$ is

$$\left. \frac{\partial^2 V}{\partial T_R^2} \right|_{T_R=T_{R0}} = -\frac{8|\mu|^2 M_{\text{pl}}}{81\iota_1^3}. \quad (45)$$

The positivity of T_R and $\left. \frac{\partial^2 V}{\partial T_R^2} \right|_{T_R=T_{R0}}$ requires $\omega_1 < 0$. The gravitino mass evaluated at $T_R = T_{R0}$ is

$$M_{3/2} \equiv \frac{e^{\frac{K}{2M_{\text{pl}}^2}}}{M_{\text{pl}}^2} |W(T)| \Big|_{T_R=T_{R0}} = \frac{1}{M_{\text{pl}}^2} \left(\frac{M_{\text{pl}}}{-3\iota_1} \right)^{3/2} \times \left| \frac{-2\omega_1 + i(\omega_2 + 2|\mu|^2 T_I)}{2\bar{\mu}} \right|. \quad (46)$$

The F term SUSY breaking scale (evaluated at $T_R = T_{R0}$) is

$$F_T|_0 \equiv e^{\frac{K}{2M_{\text{pl}}^2}} |D_T W(T)| \Big|_{T_R=T_{R0}} = \left(\frac{M_{\text{pl}}}{-3\iota_1} \right)^{3/2} \times \left| \frac{i\mu}{2\omega_1} (\omega_2 + 2|\mu|^2 T_I) \right|, \quad (47)$$

while the D term SUSY breaking scale (evaluated at $T_R = T_{R0}$) is

$$\left. \frac{1}{2} g^2 \xi^2 \right|_0 = -\frac{M_{\text{pl}} |\mu|^4}{9\omega_1} = -\frac{M_{\text{pl}} |\mu|^2}{9\iota_1}. \quad (48)$$

5 A short summary of total potentials and required tools for inflation analysis

5.1 Suppose $\rho \neq 3$.

5.1.1 Total potentials

By using Eq.(3), (27), (30) and Table 2, the total potentials (normalized by $|\mu|^2$) are given by $V = V_F + V_D$, where

$$\frac{V_F(T_R, T_I)}{|\mu|^2} = \frac{1}{M_{\text{pl}}^2} \left(\frac{M_{\text{pl}}}{2T_R} \right)^\rho \left\{ (\rho - 3) \left[\frac{(\iota_1^2 + \iota_2^2)}{4} + \iota_2 T_I + T_I^2 \right] + (\rho - 5) \iota_1 T_R + \frac{(\rho^2 - 7\rho + 4)}{\rho} T_R^2 \right\}, \quad (49)$$

and

$$\frac{V_D}{|\mu|^2} = \frac{g^2 \xi^2}{2|\mu|^2} = \frac{\iota_1}{\rho M_{\text{pl}}} \left(\frac{(\rho^2 - 7\rho + 4) M_{\text{pl}}}{-(\rho - 3) \rho \iota_1} \right)^{\rho-1}, \quad (50)$$

if $\omega_1 > 0$ and $3 < \rho < \frac{7+\sqrt{33}}{2}$, or

$$\frac{V_D}{|\mu|^2} = \frac{g^2 \xi^2}{2|\mu|^2} = \frac{3\iota_1^2}{M_{\text{pl}}^2 (\rho - 2)^2} \left(\frac{(\rho - 2) M_{\text{pl}}}{-\rho \iota_1} \right)^\rho. \quad (51)$$

if $\omega_1 < 0$ and $\rho > 3$.

5.1.2 SUGRA Lagrangian setup

We are going to find the corresponding adiabatic and iso-curvature perturbation for double field models. During inflation, since the non-zero vacuum expectation values of fermions break the Lorentz symmetry, which is not physical during inflation, we assume that only bosons contribute to the background of inflation dynamics. Hence, we consider the bosonic part of the Lagrangian, which is given by [35]

$$\mathcal{L} = \sqrt{-g} \mathcal{L}_{\text{SUGRA}} = \sqrt{-g} \left[\frac{M_{\text{pl}}^2}{2} R - K_{i\bar{j}} \nabla_\mu \phi^i \nabla^\mu \bar{\phi}^{\bar{j}} - V \right], \quad (52)$$

where $V = V_F + V_D$ while V_F and V_D are F term potential and D term potential respectively. The kinetic term in $\mathcal{L}_{\text{SUGRA}}$ can be written as

$$K_{i\bar{j}} \nabla_\mu \phi^i \nabla^\mu \bar{\phi}^{\bar{j}} = \frac{\rho M_{\text{pl}}^2}{(T + \bar{T})^2} \nabla_\mu T \nabla^\mu \bar{T} = \frac{\rho M_{\text{pl}}^2}{4T_R^2} (\nabla_\mu T_R \nabla^\mu T_R + \nabla_\mu T_I \nabla^\mu T_I). \quad (53)$$

If we treat \mathcal{L} in Eq.(52) in the Jordan frame, by Eq.(78), we obtain

$$f(\phi^I) = f(\phi^1, \phi^2) = \frac{1}{2} M_{\text{pl}}^2, \quad \phi^1 = T_R, \quad \phi^2 = T_I, \quad \tilde{\mathcal{G}}_{IJ} = \frac{\rho M_{\text{pl}}^2}{2T_R^2} \delta_{IJ}, \quad (54)$$

for all $I, J \in \{1, 2\}$. Since $f(\phi^I)$ is a constant, the metric in the field space in the Jordan frame $\tilde{\mathcal{G}}_{IJ}$ is the same as that in the Einstein frame \mathcal{G}_{IJ} . Thus, The conformal factor becomes

$$\Omega^2 = 1, \quad (55)$$

and the metric of the field space in the Einstein frame is

$$\mathcal{G}_{IJ} = \frac{\rho M_{\text{pl}}^2}{2T_R^2} \delta_{IJ}. \quad (56)$$

We expand the fields to the first order around its classical background values

$$T_R(x^\mu) = T_{Rb}(t) + \delta T_R(x^\mu), \quad \text{and} \quad T_I(x^\mu) = T_{Ib}(t) + \delta T_I(x^\mu), \quad (57)$$

The norm of the velocity vector is given by the background components of the fields as follows

$$\dot{\sigma}^2 = \mathcal{G}_{IJ} \dot{\phi}^I \dot{\phi}^J = \frac{\rho M_{\text{pl}}^2}{2T_{Rb}^2} (\dot{T}_{Rb}^2 + \dot{T}_{Ib}^2) \Rightarrow \dot{\sigma} = \frac{M_{\text{pl}}}{|T_{Rb}|} \sqrt{\frac{\rho}{2}} \sqrt{\dot{T}_{Rb}^2 + \dot{T}_{Ib}^2}, \quad (58)$$

where the norm $\dot{\sigma}$ is defined to be positive. Since the background components of fields depend on cosmic time t only, we can easily obtain the Laplacian as

$$\square \phi = -(\ddot{\phi} + 3H\dot{\phi}), \quad \forall \phi \in \{T_{Rb}, T_{Ib}\}, \quad (59)$$

and hence the equations of motion (E.O.M.)s of T_{Rb} and T_{Ib} are given by

$$\begin{aligned} -\left(\ddot{T}_{Rb} + 3H\dot{T}_{Rb}\right) - \left(\frac{-1}{T_{Rb}}\dot{T}_{Rb}^2 + \frac{1}{T_{Rb}}\dot{T}_{Ib}^2\right) - \frac{2T_{Rb}^2}{\rho M_{\text{pl}}^2} V_{T_R}|_b &= 0, \\ -\left(\ddot{T}_{Ib} + 3H\dot{T}_{Ib}\right) - \left(\frac{-1}{T_{Rb}}\dot{T}_{Rb}\dot{T}_{Ib} - \frac{1}{T_{Rb}}\dot{T}_{Rb}\dot{T}_{Ib}\right) - \frac{2T_{Rb}^2}{\rho M_{\text{pl}}^2} V_{T_I}|_b &= 0, \end{aligned} \quad (60)$$

where $V_{T_R}|_b$ and $V_{T_I}|_b$ are the first derivatives of the potential with respect to T_R and T_I evaluated at the background respectively and the dot over T_{Rb} and T_{Ib} means the derivatives of the corresponding background fields with respect to cosmic time t .

5.2 Suppose $\rho = 3$.

5.2.1 Total potentials and slow-roll parameters

Note that the total potential (normalized by $|\mu|^2$) are given by

$$\frac{V(T_R)}{|\mu|^2} = \frac{-M_{\text{pl}}}{8T_R^3} \left(\frac{8}{3}T_R^2 + 2T_{R\ell_1} \right) - \frac{M_{\text{pl}}}{9\ell_1}, \quad (61)$$

which is independent of T_I . Hence,

$$\frac{\partial V}{\partial T_I} = \frac{\partial^2 V}{\partial T_R \partial T_I} = \frac{\partial^2 V}{\partial T_I \partial T_R} = \frac{\partial^2 V}{\partial T_I^2} = 0, \quad \forall (T_R, T_I) \in \mathbb{R}^2. \quad (62)$$

5.2.2 Equations of motion

The bosonic part of Lagrangian and the kinetic terms of $\rho = 3$ case are given by Eq.(60). Hence, the E.O.M.s of T_R and T_I become

$$\begin{aligned} -\left(\ddot{T}_{Rb} + 3H\dot{T}_{Rb}\right) - \left(\frac{-1}{T_{Rb}}\dot{T}_{Rb}^2 + \frac{1}{T_{Rb}}\dot{T}_{Ib}^2\right) - \frac{2T_{Rb}^2}{\rho M_{\text{pl}}^2} V_{T_R}|_b &= 0, \\ -\left(\ddot{T}_{Ib} + 3H\dot{T}_{Ib}\right) - \left(\frac{-1}{T_{Rb}}\dot{T}_{Rb}\dot{T}_{Ib} - \frac{1}{T_{Rb}}\dot{T}_{Rb}\dot{T}_{Ib}\right) &= 0. \end{aligned} \quad (63)$$

We will adopt Eq. (63) to evaluate their corresponding evolutions.

6 Numerical calculations

6.1 Suppose $\rho \neq 3$.

$ \mu /M_{\text{pl}}^2$	N_{hc}	$T_R'(N=0)$	$T_I'(N=0)$
3×10^{-4}	0	10^{-5}	10^{-5}

Table 4: Fixed values for numerical calculations

We are going to show the feasible parameters for inflation, and the corresponding β_{iso} and $\cos(\Delta)$ are evaluated based on that parameters. Recall β_{iso} and $\cos(\Delta)$ are given by

$$\beta_{\text{iso}} = \frac{T_{SS}(N_{\text{hc}}, N_{\text{end}})^2}{1 + T_{SS}(N_{\text{hc}}, N_{\text{end}})^2 + T_{RS}(N_{\text{hc}}, N_{\text{end}})^2}, \quad (64)$$

$$\cos(\Delta) = \frac{T_{\mathcal{RS}}(N_{\text{hc}}, N_{\text{end}})^2}{\sqrt{1 + T_{\mathcal{RS}}(N_{\text{hc}}, N_{\text{end}})^2}} \quad (65)$$

First, we find the initial conditions based on the constraints of ϵ_V , η_V , n_s , V_{hc} listed in Table 1 and the initial conditions listed on Table 4, and extract some points for path evolution. Next, we set some fixed parameters as shown in Table 4, while various sets of parameters are listed in Table 5 for $\rho = 4$, Table 6 for $\rho = 5$ and Table 7 for $\rho = 6$ respectively.

6.1.1 Suppose $\omega_1 > 0$, $3 < \rho < \frac{7+\sqrt{33}}{2}$.

In Figure 1, we show the possible positive values of $T_{R_{\text{hc}}}$ ⁵, $T_{I_{\text{hc}}}$ and ι_2/ι_1 based on the Planck observation constraints listed in Table 1 at various $\rho = 4, 5, 6$. The "C" shape tube regions gradually change the color from red to green as ι_1 gradually increases with a constant increment (For details, please refer to the description of Figure 1). We extract some of the possible parameters satisfying the e-folding constraints $50 \leq N_{\text{end}} - N_{\text{hc}} \leq 60$ as listed in Table 5, 6 and 7, and their corresponding evolution paths are plotted in Figure 2. The colors correspond to the counterparts of the paths shown in Figure 2. One can see that for $\rho = 4$, the background fields move towards their corresponding minimum point (dS vacuum point)⁶ in a nearly straight line, turn to the minimum point with a larger turn rate and then oscillate around the minimum point. As ρ increases gradually up to 6, the background fields greatly turn in the initial stage, move towards their corresponding minimum point and finally oscillate around the minimum point.

Next, in Figure 3, we can see the evolutions of ϵ and $\eta_{\sigma\sigma}$ of all the listed parameter sets in Table 5, 6 and 7. Basically, starting from very small positive values, all the ϵ (dotted) lines evolve and keep at a close-to-zero value, surge to 3 after 50 e-folding and then oscillate between 0 and 3. Also, $\eta_{\sigma\sigma}$ (solid) lines start from a value very close to zero, evolve around zero and then sharply increase at the end of inflation. That means the background fields roll slowly initially and then run at an increasing rate, which is consistent with the mechanism of inflation. In Figure 4, after dropping sharply from a large positive value to a small positive value, the effective mass square of the entropy perturbation $(\mu_s/H)^2$, which is given by Eq.(113), remains light and physical. This shows that the trajectories roll from the plateau. Since μ_s^2 is related to the curvature of the potential in the direction orthogonal to the trajectory, light mass square means the curvature orthogonal to the trajectory is small at the initial stage. When the background fields roll off the ridge and reach 50 e-folding, the entropy mass square largely grows because the curvature orthogonal to the trajectory is large and the turn rate becomes significant as the background field oscillates around their corresponding minimum points.

6.1.2 Suppose $\omega_1 < 0$, $\rho > 3$.

Similar to the cases $\omega_1 > 0$, in Figure 7, we show the possible positive values of $T_{R_{\text{hc}}}$, $T_{I_{\text{hc}}}$ and ι_2/ι_1 based on the Planck observation constraints listed in Table 1 at various $\rho = 4, 5, 6$. The "C" shape tube regions gradually change the color from red to green as ι_1 gradually decreases with a constant increment (For details, please refer to the description of Figure 7). We also extract some of the possible parameters satisfying the e-folding constraints $50 \leq N_{\text{end}} - N_{\text{hc}} \leq 60$

⁵In this paper, we assume the first horizon crossing is the start of inflation. The subscript "hc" means "horizon crossing".

⁶One can find their corresponding minimum point $(T_{R_{\text{end}}}, T_{I_{\text{end}}})$ in Table 5, 6 and 7. Here "dS" means "dS vacuum".

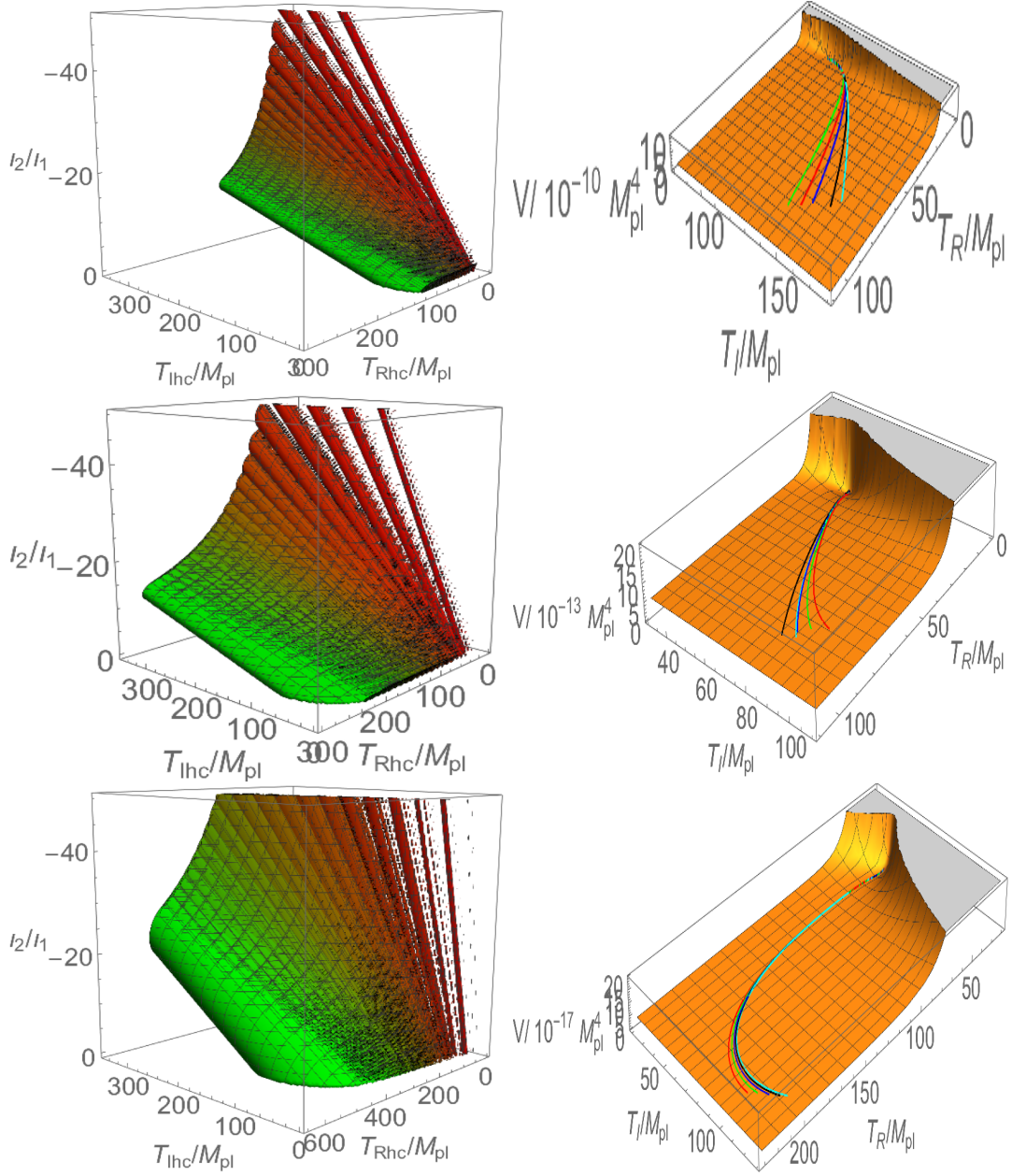


Figure 1: Left: Regions of possible values of T_{Rhc} , T_{Lhc} l_2/l_1 for inflation based on the constraints listed in Table 1 at various integers ρ , a fixed $|\mu| = 3 \times 10^{-4} M_{pl}^2$ and $\omega_1 > 0$ ($\iota_1 > 0$). Each "C" shaped tube moves from red color to green color as ι_1 increases. Please pay attention to the direction of magnitude of each axis in each graph. 1st row: $\rho = 4$, from $\iota_1 = 9M_{pl}$ (red) to $\iota_1 = 49M_{pl}$ (green) with an increment of $2M_{pl}$; 2nd row: $\rho = 5$, from $\iota_1 = 6M_{pl}$ (red) to $\iota_1 = 46M_{pl}$ (green) with an increment of $2M_{pl}$; 3rd row: $\rho = 6$, from $\iota_1 = 1M_{pl}$ (red) to $\iota_1 = 21M_{pl}$ (green) with an increment of $1M_{pl}$. (These regions are restricted by Table 1 only without the e-folding constraints $50 \leq N_{end} - N_{hc} \leq 60$.) Right: The trajectories of background fields on the potential surface. 1st row: $\rho = 4$, 2nd row: $\rho = 5$, 3rd row: $\rho = 6$. Various colors of the paths correspond to the parameter sets listed on Table 5, 6 and 7 respectively.

as listed in Table 8, 9 and 10, and their corresponding evolution paths are plotted in Figure 8. One can see that for $\rho = 4$, the paths move towards their corresponding minimum point (dS vacuum point) in a nearly a straight line, turn to the minimum point with a larger turn rate and then oscillate around the minimum point. However, the extent of turning is smaller than that of the evolution paths at $\omega_1 > 0$ and $\rho = 4$. As ρ increases gradually up to 6, the paths

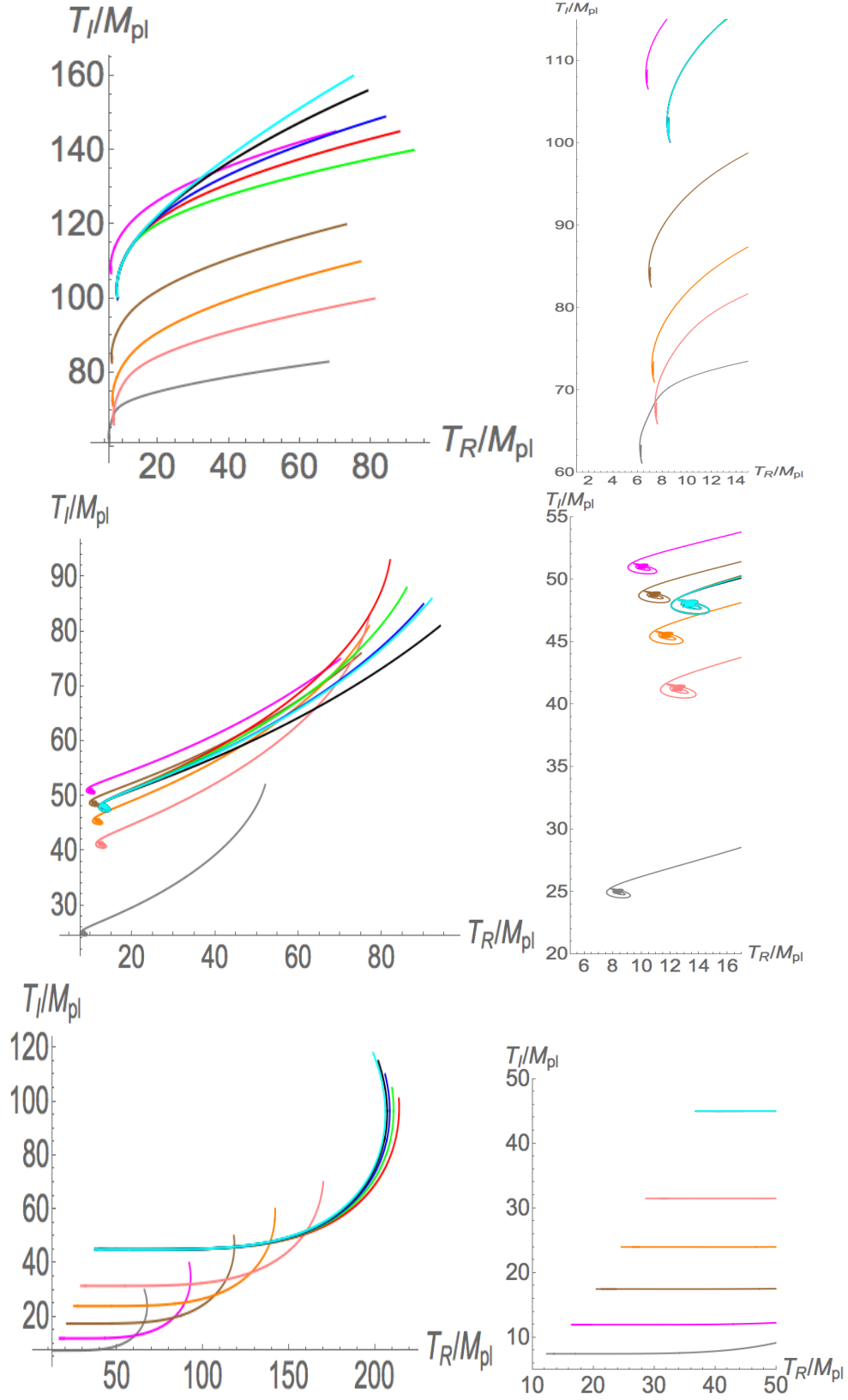


Figure 2: Evolution paths of inflation dynamics at $\omega_1 > 0$ ($\iota_1 > 0$). 1st row: $\rho = 4$, 2nd row: $\rho = 5$, 3rd row: $\rho = 6$. Various colors refer to various parameter sets listed on Table 5, 6 and 7 correspondingly.

change its shape into the form like turning greatly in the initial stage, moving towards their corresponding minimum point and finally oscillating around the minimum point.

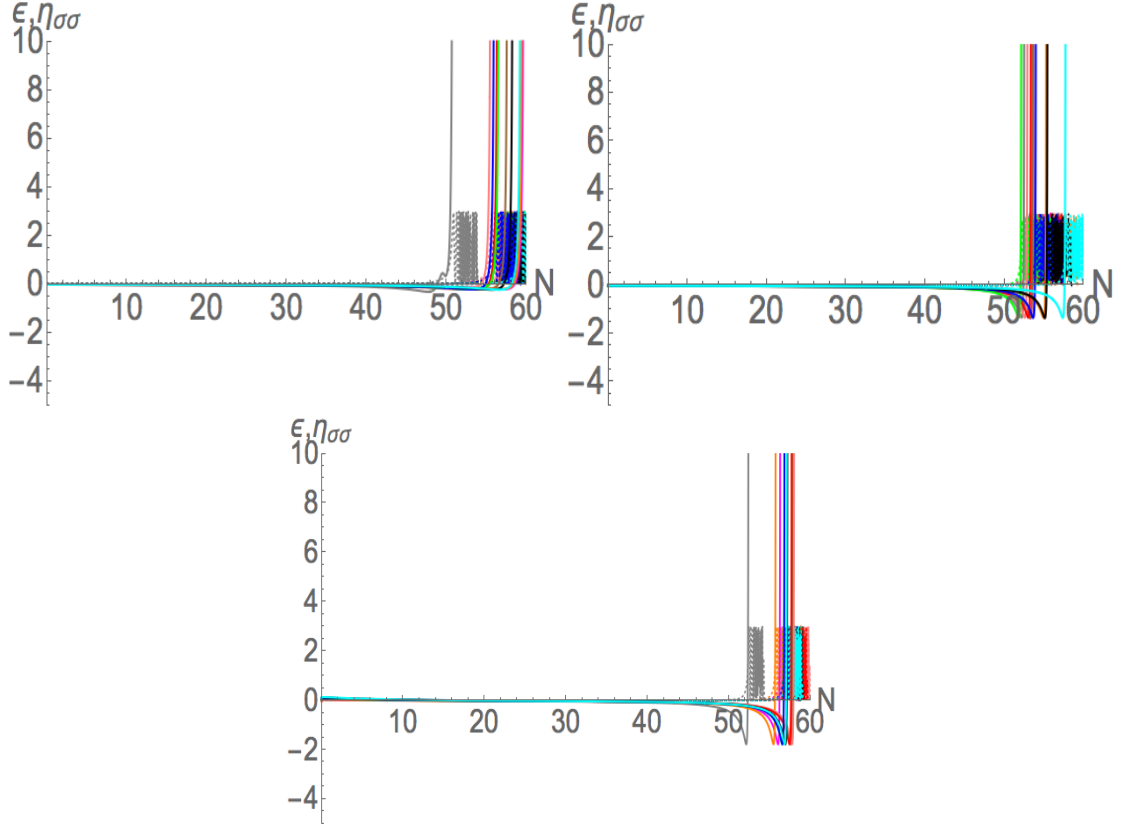


Figure 3: Evolutions of slow-roll parameters ϵ and $\eta_{\sigma\sigma}$ at $\omega_1 > 0$ ($\iota_1 > 0$). 1st row: $\rho = 4$, 2nd row: $\rho = 5$, 3rd row: $\rho = 6$. Various colors refer to various parameter sets listed on Table 5, 6 and 7 correspondingly. Dotted lines represent the evolutions of ϵ while the solid lines represent the counterpart of $\eta_{\sigma\sigma}$.

Next, in Figure 9, we can see the evolutions of ϵ and $\eta_{\sigma\sigma}$ of all the listed parameter sets in Table 8, 9 and 10. Basically, starting from very small positive values, all the ϵ (dotted) lines evolve and keep at a close-to-zero value, surge to 3 after 50 e-folding and then oscillate between 0 and 3. Also, $\eta_{\sigma\sigma}$ lines start from a value very close to zero, evolve around zero and then sharply increase at the end of inflation. In Figure 4, after dropping sharply from a large positive value to a small positive value, the effective mass square of the entropy perturbation $(\mu_s/H)^2$ remains light and physical. This shows that the trajectory rolls from the plateau, where the field space curvature orthogonal to the trajectory is small in the initial stage, to the minimum point, where the entropy mass square largely grows.

6.2 Suppose $\rho = 3$.

The total potential is given by Eq.(61). The possible initial T_{Rhc} , $\iota_1 = \omega_1/|\mu|^2$ and $|\mu|$ are shown in Figure 13. Also, the parameters of possible inflation are given by Table 11. The evolutions of the background fields T_R and T_I are evaluated by their E.O.M.s Eq. (63). Basically, the paths are straight lines from the initial starting points. Next, for slow-roll parameters as shown in Figure 15, starting from a value very close to zero, they keep its low value and become significant after 50 e-folding, which is consistent with the usual inflation mechanism. Apart from these, from Figure 16, we can see that turn rates drop rapidly and keep nearly zero as the background fields roll off the ridge. This shows that the fields turn for a little while and roll straight off the ridge. Furthermore, in Figure 18, we can know that the evolutions of the effective mass square of the entropy perturbation $(\mu_s/H)^2$ remains nearly zero.

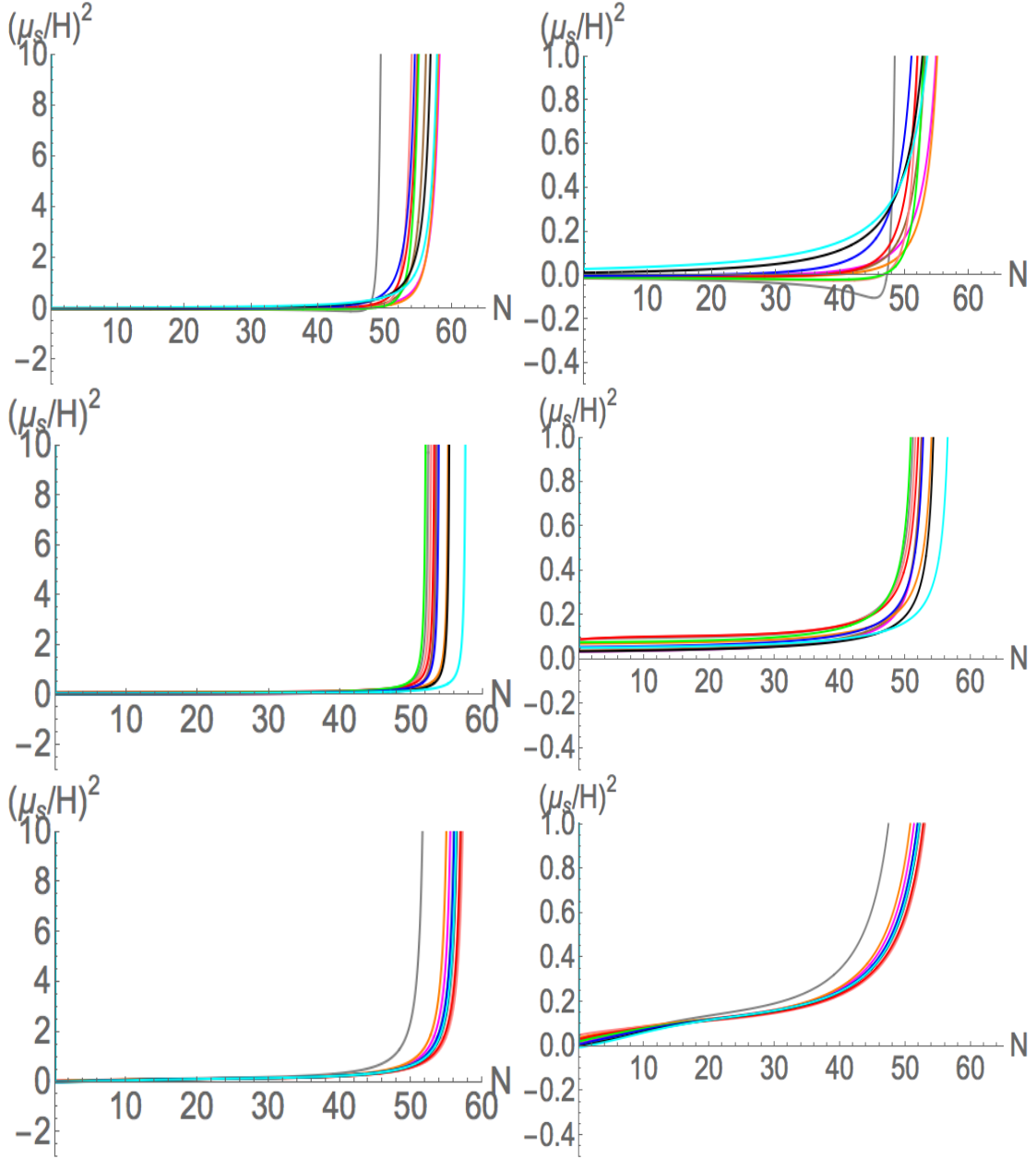


Figure 4: Square of effective mass per Hubble parameter $(\mu_s/H)^2$ at $\omega_1 > 0$ ($\iota_1 > 0$). 1st row: $\rho = 4$, 2nd row: $\rho = 5$, 3rd row: $\rho = 6$. The graphs on the right hand side (R.H.S.) are the close shots of that on the left hand side (L.H.S.) near zero. Various colors refer to various parameter sets listed on Table 5, 6 and 7 correspondingly.

7 Discussion

7.1 The scale of the potential

Referring to Figure 1 and 7, one can see that the evolution paths exist at different energy scales. In fact, there are two main parameters affecting the potential scale. One is $|\mu|$, and another is ρ . Referring to Eq.(49), (50) and (51), one can see that the potential is directly proportional to $|\mu|^2$, while the powers of $\left(\frac{M_{\text{Pl}}}{2T_R}\right)^\rho$ in Eq.(49), $\left(\frac{(\rho^2-7\rho+4)M_{\text{Pl}}}{-(\rho-3)\rho\iota_1}\right)^{\rho-1}$ in Eq.(50) and $\left(\frac{(\rho^2-7\rho+4)M_{\text{Pl}}}{-(\rho-3)\rho\iota_1}\right)^{\rho-1}$ in Eq.(51) show ρ is related to the power of some field values and param-

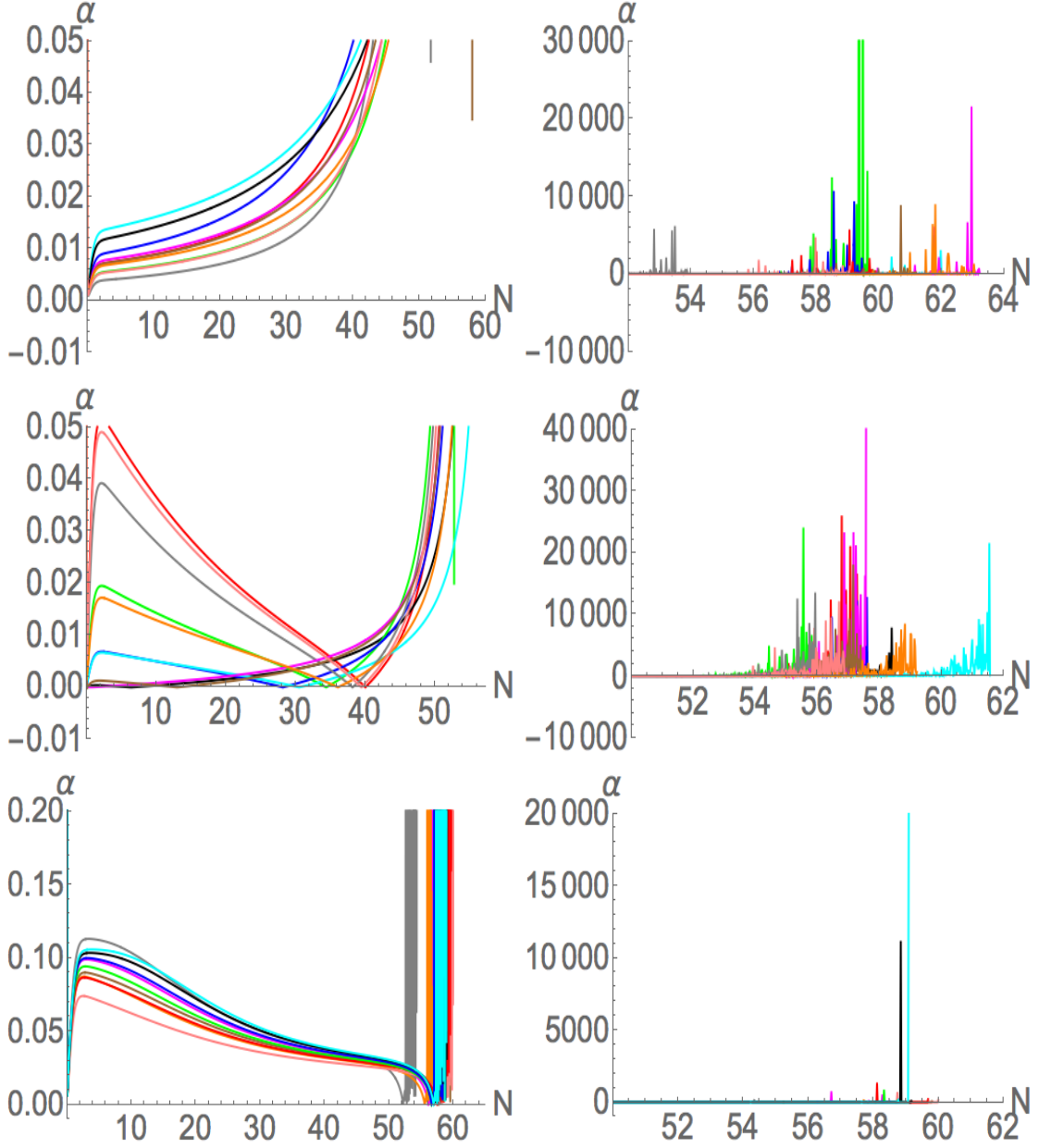


Figure 5: 2 times of turn rate per Hubble parameter $\alpha = 2\omega/H$ at $\omega_1 > 0$ ($\iota_1 > 0$). 1st row: $\rho = 4$, 2nd row: $\rho = 5$, 3rd row: $\rho = 6$. Left graphs show the overall evolutions, while right graphs focus on the changes at the end of inflation. Various colors refer to various parameter sets listed on Table 8, 9 and 10 correspondingly.

ters. Since $|\mu|$ is held in a fixed scale $O(10^{-4}) M_{\text{pl}}$, the difference lies in various ρ . Since the scale of field values is $O(10^2) M_{\text{pl}}$, the potential scale decreases by 10^{-2} times as ρ increases by 1.

7.2 Turn rate for $\rho \neq 3$

In Figure 2 and 8, one can see that there are path patterns with various extent of turning. This can be tracked by Figure 5 (and 11) respectively. For example, for $\omega_1 > 0$ and $\rho = 4$, when the background fields roll off from the initial point, there is no rigorous turning until the end of inflation, leading to the evolution of $2\omega/H$ close to zero. As they gradually approach to their corresponding minimum points, Hubble scale H reduces gradually and the turning

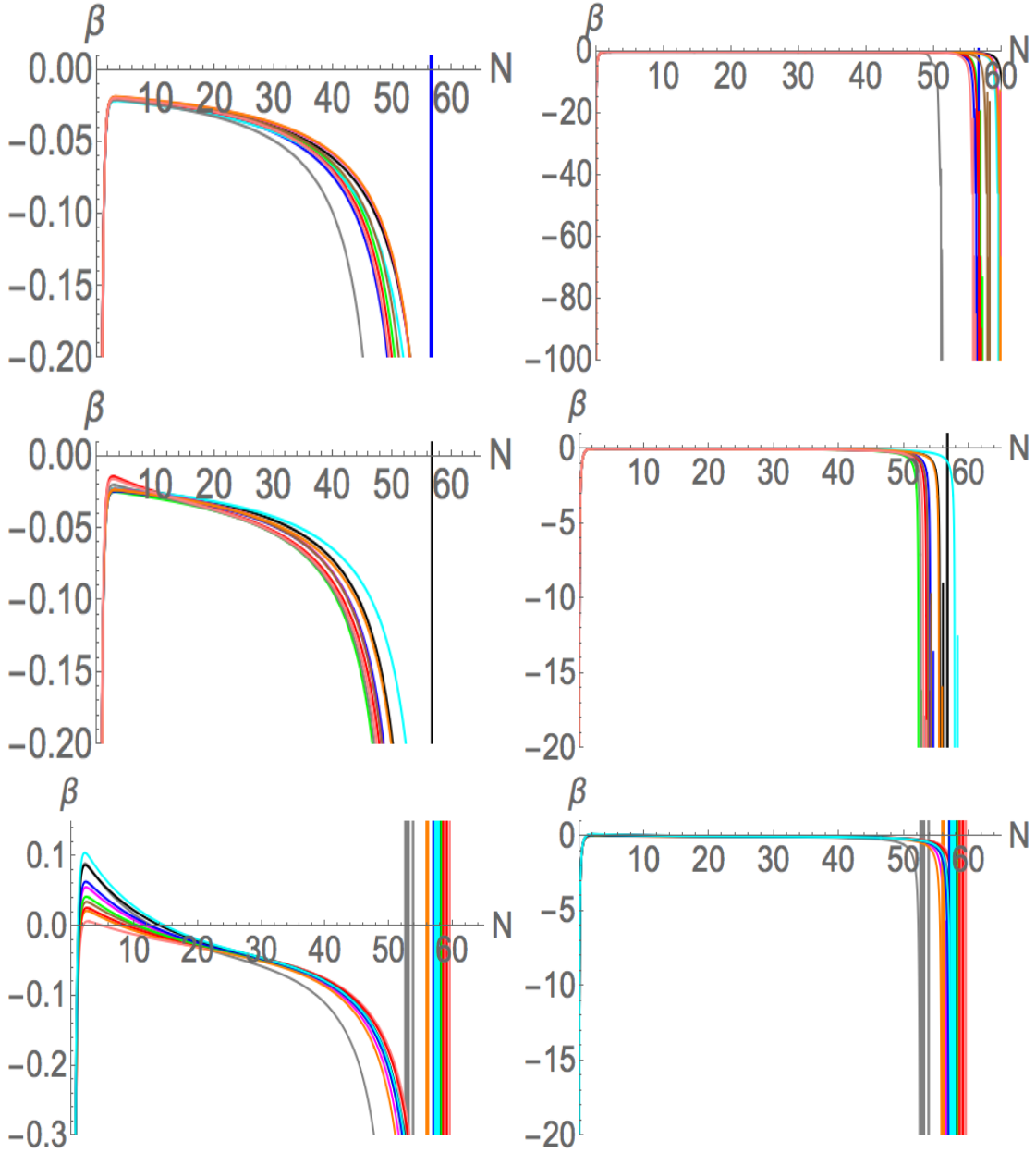


Figure 6: β at $\omega_1 > 0$ ($\iota_1 > 0$). 1st row: $\rho = 4$, 2nd row: $\rho = 5$, 3rd row: $\rho = 6$. The graphs on the right hand side (R.H.S.) are the close shots of that on the left hand side (L.H.S.). Various colors refer to various parameter sets listed on Table 8, 9 and 10 correspondingly.

becomes rigorous, resulting in the gradual rise of $2\omega/H$. Finally, when they oscillate around their minimum points, the turning becomes sharply rigorous, leading to the sudden surge of $2\omega/H$. Similar arguments can also be made for other cases by tracking the evolution paths and the variations of $2\omega/H$.

7.3 The turning for $\rho = 3$ and the afterward evolution

From Figure 18, since the initial speeds of background fields have the small scale $10^{-5}M_{\text{pl}}$, it is not obvious to see the turning. Hence, we demonstrate the inflation path with the greatest possible initial speed of T_I . The parameter sets are shown in Table 12 and their corresponding evolution paths are shown in Figure 19. We can significantly see that the background fields move along T_I a little while and turn towards the decreasing T_R direction. However, $\alpha(N)$

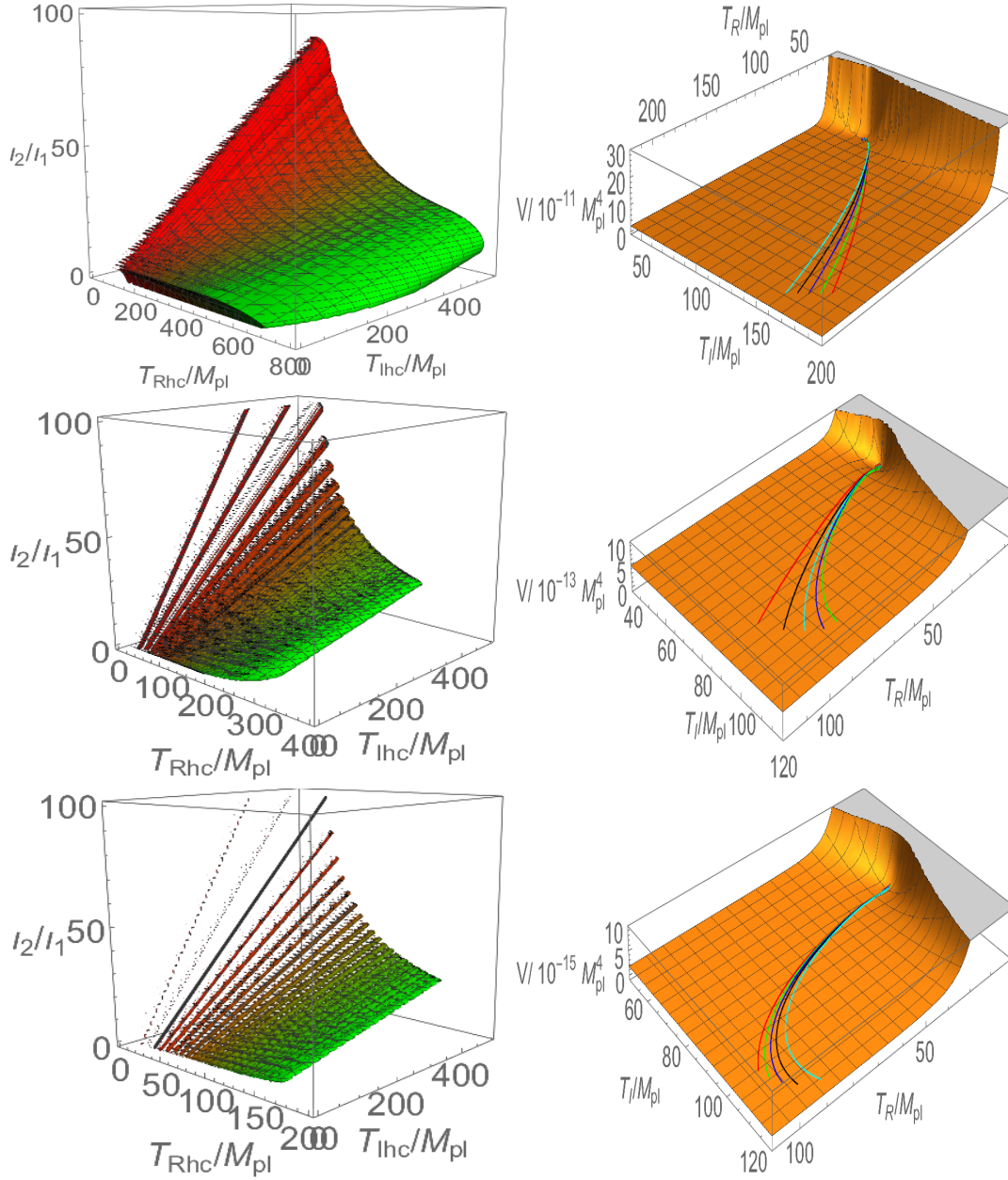


Figure 7: Left: Regions of possible values of T_{Rhc} , T_{Lhc} l_2/l_1 for inflation based on the constraints listed in Table 1 at various integers ρ , a fixed $|\mu| = 3 \times 10^{-4} M_{pl}^2$ and $\omega_1 < 0$ ($\iota_1 < 0$). Each "C" like cylinder moves from red color to green color as ι_1 increases. Please pay attention to the direction of magnitude of each axis in each graph. 1st row: $\rho = 4$, from $\iota_1 = -12M_{pl}$ (red) to $\iota_1 = -52M_{pl}$ (green) with an increment of $2M_{pl}$; 2nd row: $\rho = 5$, from $\iota_1 = -6M_{pl}$ (red) to $\iota_1 = -46M_{pl}$ (green) with an increment of $2M_{pl}$; 3rd row: $\rho = 6$, from $\iota_1 = -6M_{pl}$ (red) to $\iota_1 = -46M_{pl}$ (green) with an increment of $2M_{pl}$. (These regions are restricted by Table 1 only without the e-folding constraints $50 \leq N_{end} - N_{hc} \leq 60$.) Right: The trajectories of background fields on the potential surface. 1st row: $\rho = 4$, 2nd row: $\rho = 5$, 3rd row: $\rho = 6$. Various colors of the paths correspond to the parameter sets listed on Table 8, 9 and 10 respectively.

is reduced as the initial speed of background fields increases. That is because the turn rate per Hubble parameter is mainly inversely proportional to the resultant field rate. Hence, even though it is not significant to see the turning in the field evolution graph, the initial $\alpha(N)$ is comparatively large, and vice versa. After that, the background fields keep its T_I coordinate

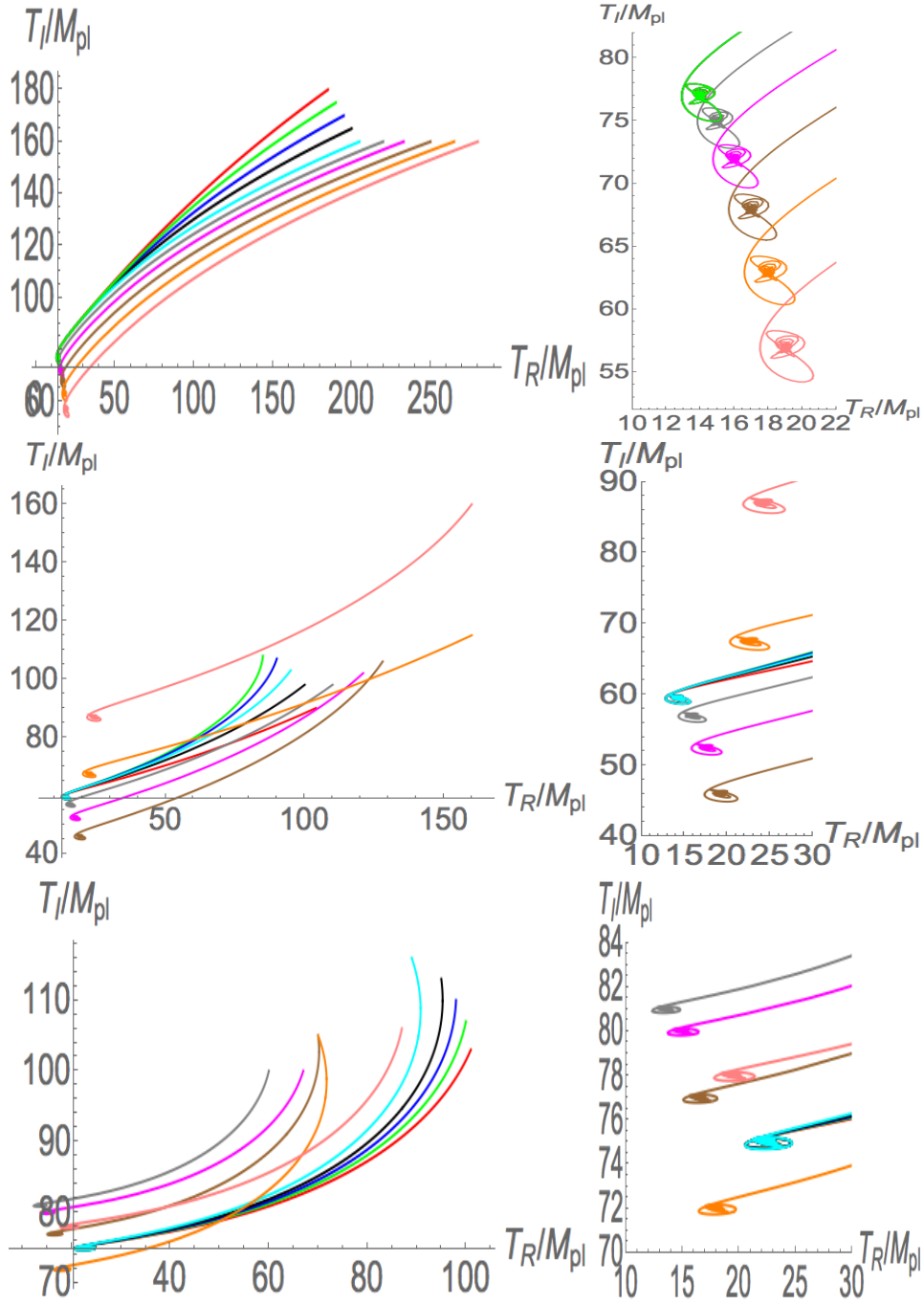


Figure 8: Evolution paths of inflation dynamics at $\omega_1 < 0$ ($\iota_1 < 0$). 1st row: $\rho = 4$, 2nd row: $\rho = 5$, 3rd row: $\rho = 6$. Various colors refer to various parameter sets listed on Table 8, 9 and 10 correspondingly.

when they continue rolling. This is because Hubble parameter and \dot{T}_R/T_R in Eq.(63) act as friction terms to stabilize the curve at a constant T_I coordinate.

7.4 The smallness of β_{iso} and $\cos(\Delta)$

To understand the smallness of β_{iso} and $\cos(\Delta)$, we should consider the reason of smallness of T_{SS} and T_{RS} , since they are related by Eq.(64) and (65). By Eq.(118) and (119) (or by Eq.(116) and (117)), we can see that T_{SS} and T_{RS} depend on the strengths of α (turn rate per Hubble parameter) and β . By Figure 5, 6, 11 and 12, we can see $\alpha(N)$ is nearly zero, while $\beta(N)$ keeps negative from N_{hc} to N_{end} . These show that T_{SS} becomes exponentially suppressed

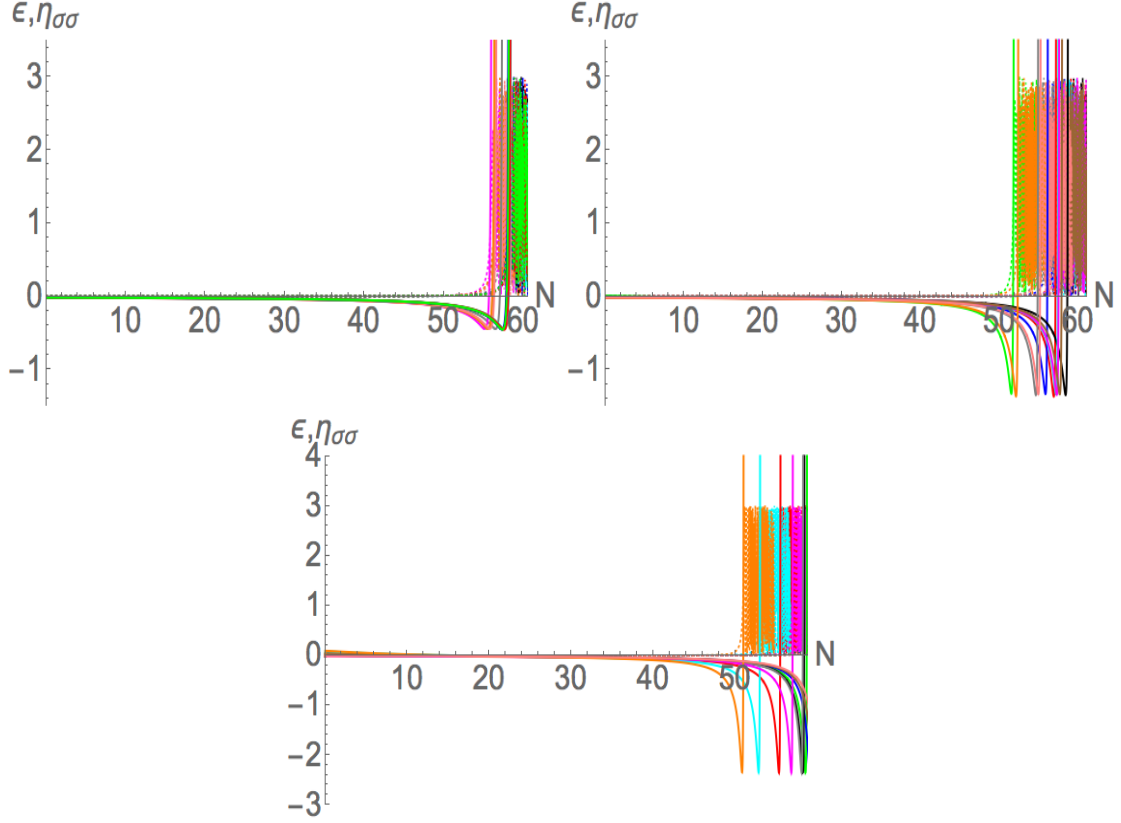


Figure 9: Evolutions of slow-roll parameters at $\omega_1 < 0$ ($\iota_1 < 0$). 1st row: $\rho = 4$, 2nd row: $\rho = 5$, 3rd row: $\rho = 6$. Various colors refer to various parameter sets listed on Table 8, 9 and 10 correspondingly. Dotted lines represent the evolutions of ϵ while the solid lines represent the counterpart of $\eta_{\sigma\sigma}$.

and there is very small contribution by each dN in the integration of $T_{\mathcal{RS}}$, leading to smallness of T_{SS} and $T_{\mathcal{RS}}$, and so are β_{iso} and $\cos(\Delta)$.

8 Conclusion

We studied the inflation dynamics of generalized dilaton-axion models with a new Fayet-Iliopoulos (FI) term not requiring gauging R-symmetry, where both dilaton T_R and its axionic partner T_I are responsible for contributing the evolution of inflation. We found that to obtain dS vacuum at the end of inflation, integer ρ in the generalized Kähler potential is constrained at different cases of ω_1 . Particularly, when $\rho = 3$, the axionic partner does not contribute to the inflation as it is absent in the total potential. We also evaluated the feasible initial conditions to produce successful inflation based on Planck observation and e-folding constraint and showed different evolution paths with various turning patterns of the background field. This shows that apart from slow roll parameters, spectral index and inflation energy scale, the change of turn rates can also be one of the fingerprints to identify the specific inflation pattern in double field model verification. Finally, we gave the predictions of iso-curvature mode contributions such as β_{iso} and $\cos \Delta$.

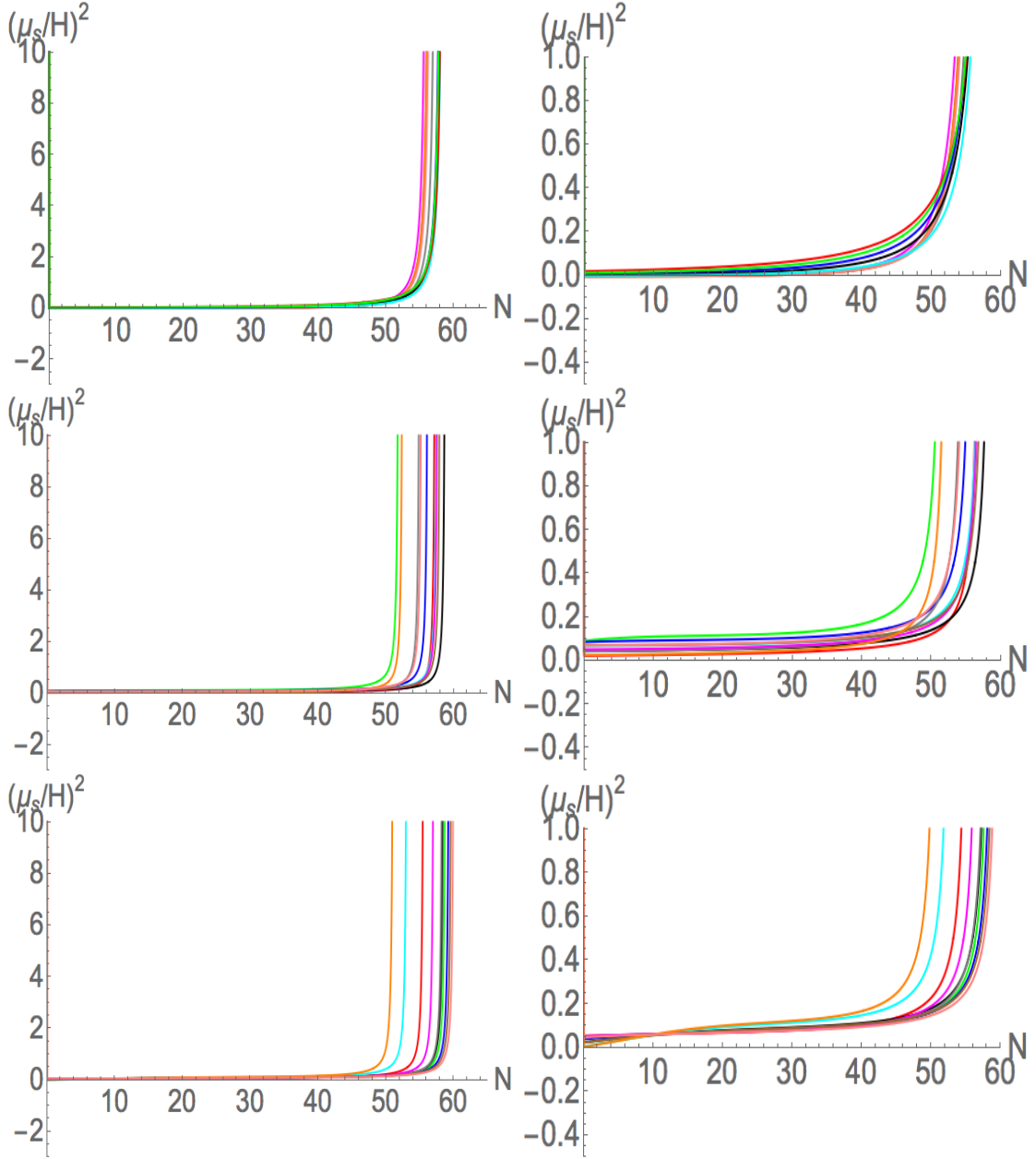


Figure 10: Square of effective mass per Hubble parameter $(\mu_s/H)^2$ at $\omega_1 < 0$ ($\iota_1 < 0$). 1st row: $\rho = 4$, 2nd row: $\rho = 5$, 3rd row: $\rho = 6$. The graphs on the right hand side (R.H.S.) are the close shots of that on the left hand side (L.H.S.) near zero. Various colors refer to various parameter sets listed on Table 8, 9 and 10 correspondingly.

9 Acknowledgement

The author thanks Prof. Hiroyuki ABE very much for suggestion and useful discussions. The author is supported by AY 2019 Scholarship for Young Doctoral Students, Waseda University.

A Christoffel symbols and curvatures of field spaces

Given that the metric of the field space in the Einstein frame is given by

$$\mathcal{G}_{IJ} = \frac{\rho M_{\text{pl}}^2}{2T_R^2} \delta_{IJ} \quad \forall I, J \in \{1, 2\}, \quad (66)$$

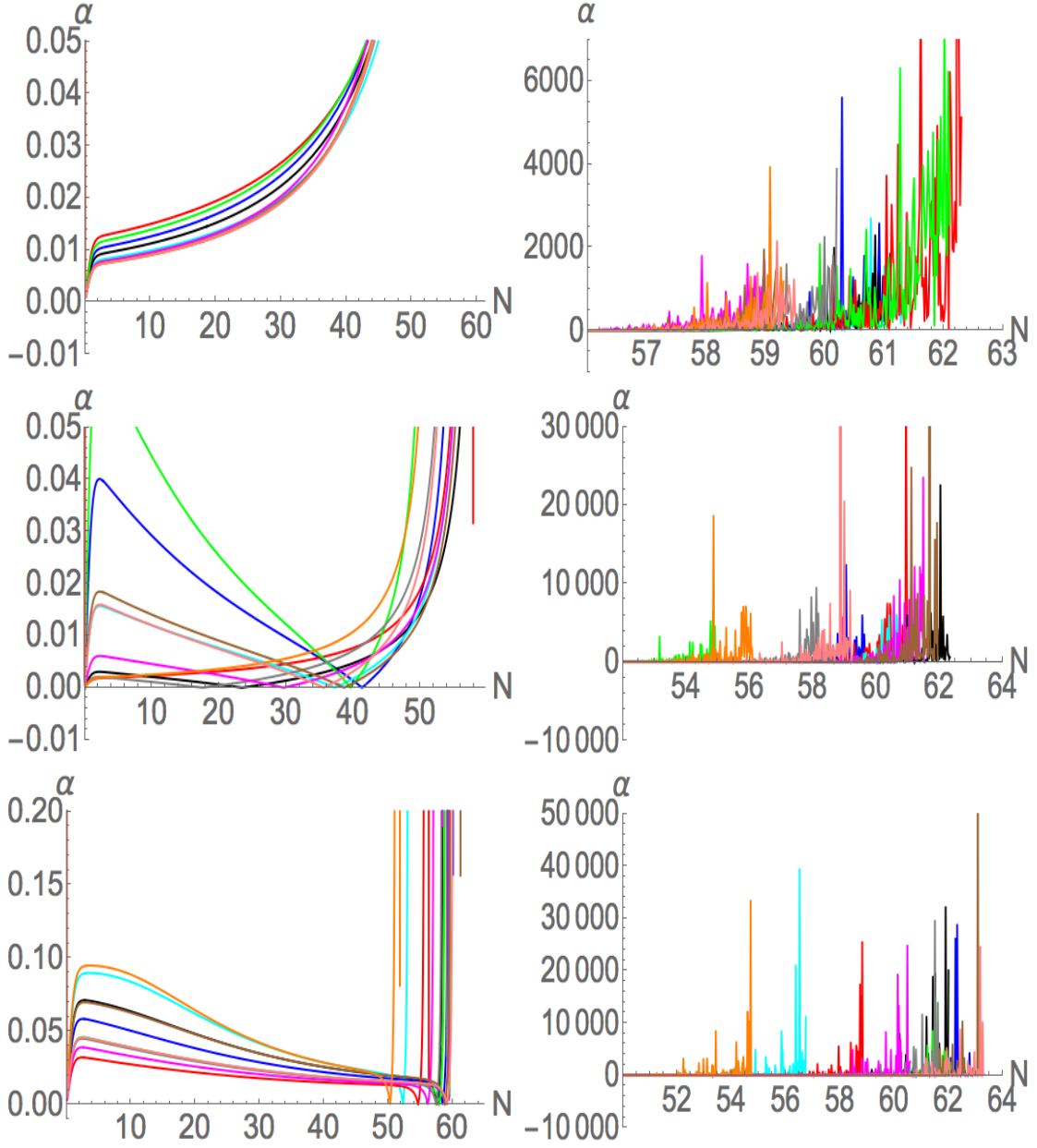


Figure 11: 2 times of turn rate per Hubble parameter $\alpha = 2\omega/H$ at $\omega_1 < 0$ ($\iota_1 < 0$). 1st row: $\rho = 4$, 2nd row: $\rho = 5$, 3rd row: $\rho = 6$. The graphs on the right hand side (R.H.S.) are the close shots of that on the left hand side (L.H.S.). Various colors refer to various parameter sets listed on Table 8, 9 and 10 correspondingly. Left graphs show the overall evolutions, while right graphs are the closed shots at the end of inflation.

the non-zero Christoffel symbols defined by

$$\Gamma_{JK}^I = \frac{1}{2} \mathcal{G}^{IL} (\mathcal{G}_{LJ,K} + \mathcal{G}_{LK,J} - \mathcal{G}_{JK,L}), \quad (67)$$

are

$$-\Gamma_{11}^1 = \Gamma_{22}^1 = -\Gamma_{12}^2 = -\Gamma_{21}^2 = \frac{1}{T_R}. \quad (68)$$

The non-zero curvature tensors defined by

$$R_{JKL}^I = \partial_K \Gamma_{JL}^I + \Gamma_{CK}^I \Gamma_{JL}^C - (\partial_L \Gamma_{JK}^I + \Gamma_{CL}^I \Gamma_{JK}^C), \quad (69)$$

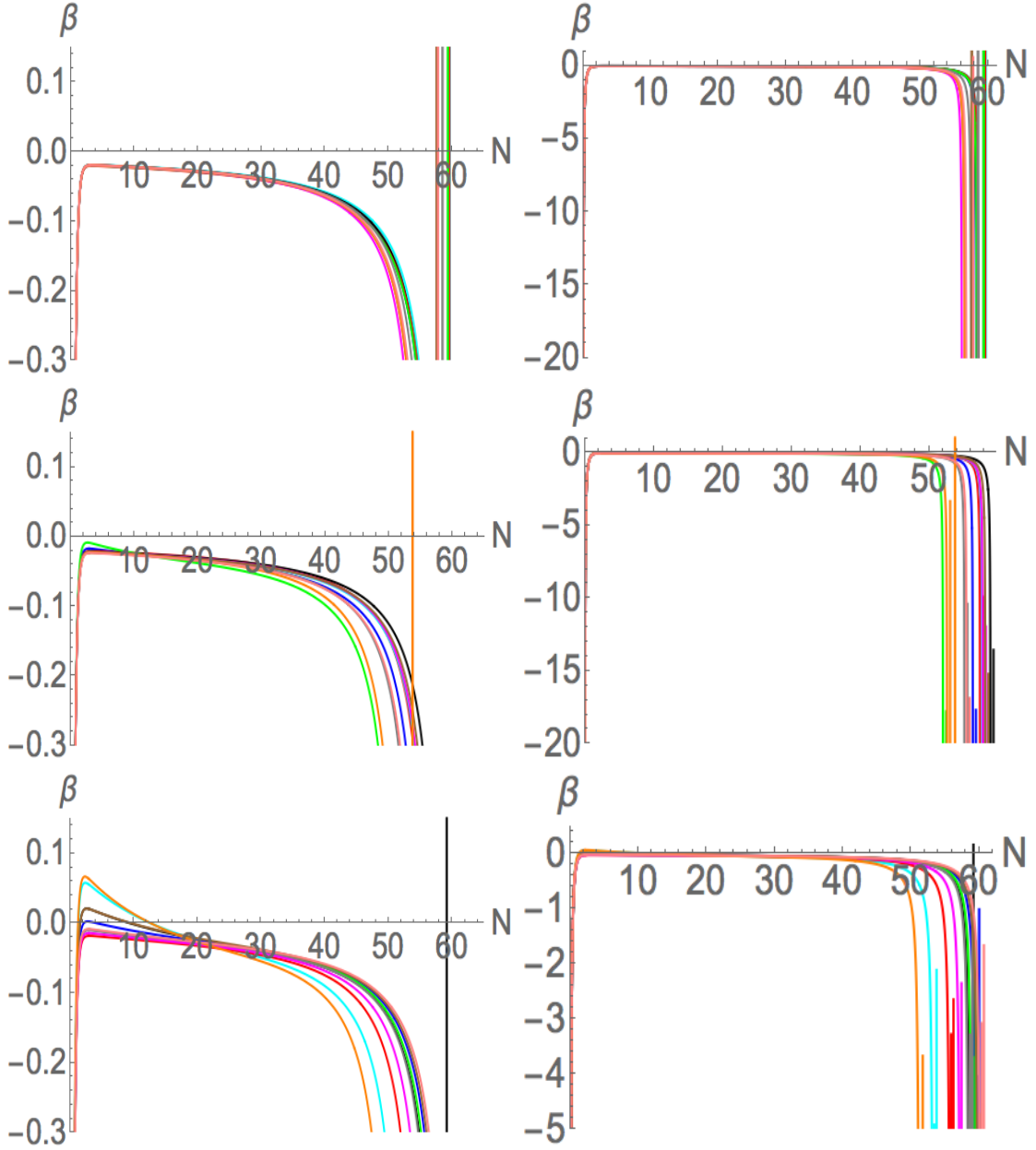


Figure 12: β at $\omega_1 < 0$ ($\iota_1 < 0$). 1st row: $\rho = 4$, 2nd row: $\rho = 5$, 3rd row: $\rho = 6$. The graphs on the right hand side (R.H.S.) are the close shots of that on the left hand side (L.H.S.). Various colors refer to various parameter sets listed on Table 8, 9 and 10 correspondingly.

are

$$-R_{212}^1 = R_{221}^1 = R_{112}^2 = -R_{121}^2 = \frac{1}{T_R^2}, \quad (70)$$

which gives the Ricci tensor defined by $R_{JL} = \mathcal{G}_I^K R_{JKL}^I = R_{JIL}^I$ as

$$R_{11} = R_{22} = -\frac{1}{T_R^2}, \quad (71)$$

and the curvature scalar, defined by $R \equiv \mathcal{G}^{IJ} R_{IJ}$, as

$$R = -\frac{4}{\rho M_{\text{pl}}^2}. \quad (72)$$

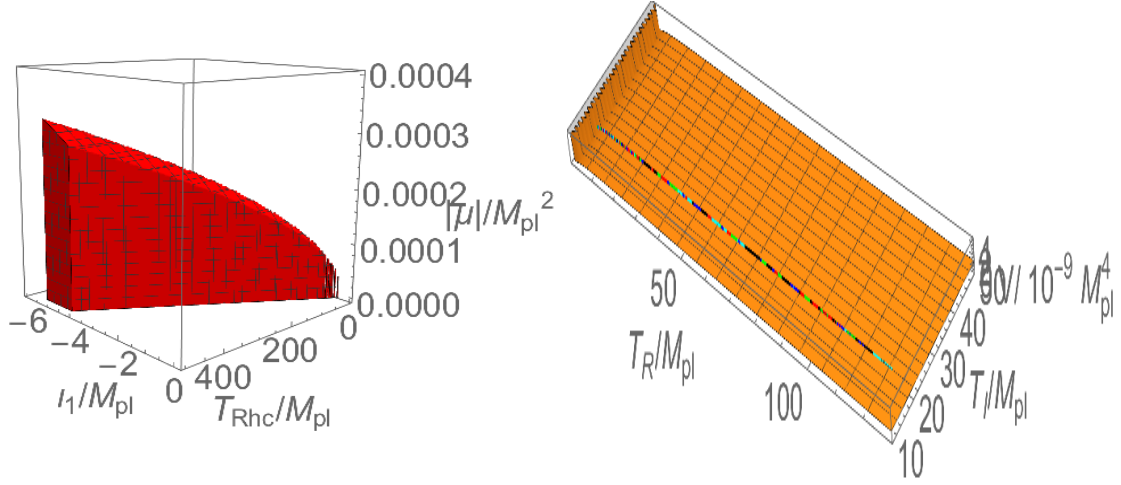


Figure 13: Left: A region of possible values of T_{Rhc}/M_{pl} , ι_1/M_{pl} and $|\mu|/M_{\text{pl}}^2$ for inflation based on the constraints listed in Table 1. Right: The evolution of background fields on the potential surface. The colors of the lines correspond to the parameter sets listed in Table 1.

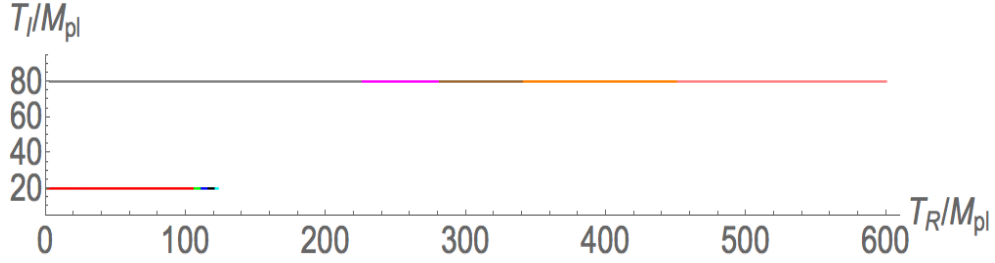


Figure 14: Evolution paths of inflation dynamics at $\rho = 3$. Various colors refer to various parameter sets listed on Table 11.

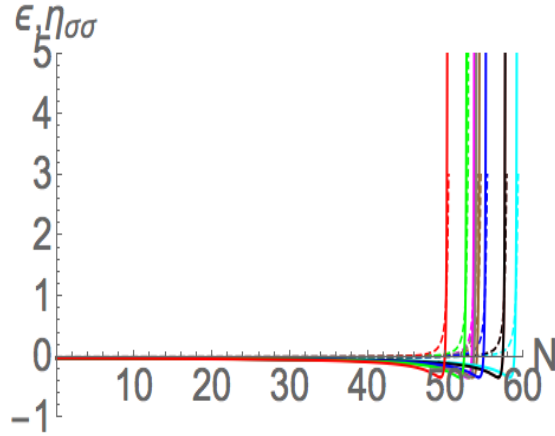


Figure 15: Evolutions of slow-roll parameters ϵ and $\eta_{\sigma\sigma}$ for $\rho = 3$. Various colors refer to various parameter sets listed on Table 11. Dotted lines represent the evolutions of ϵ while the solid lines represent the counterpart of $\eta_{\sigma\sigma}$.

B A formalism of Double Field Inflation

In this section, we follow the derivation in [6] and [9]. Note that in the Jordan frame, the Lagrangian is

$$S_{\text{Jordan}} = \int d^4x \sqrt{-\tilde{g}} \left[f(\phi^I) \tilde{R} - \frac{1}{2} \tilde{G}_{IJ} \tilde{g}^{\mu\nu} \tilde{\nabla}_\mu \phi^I \tilde{\nabla}_\nu \phi^J - \tilde{V}(\phi^I) \right]. \quad (73)$$

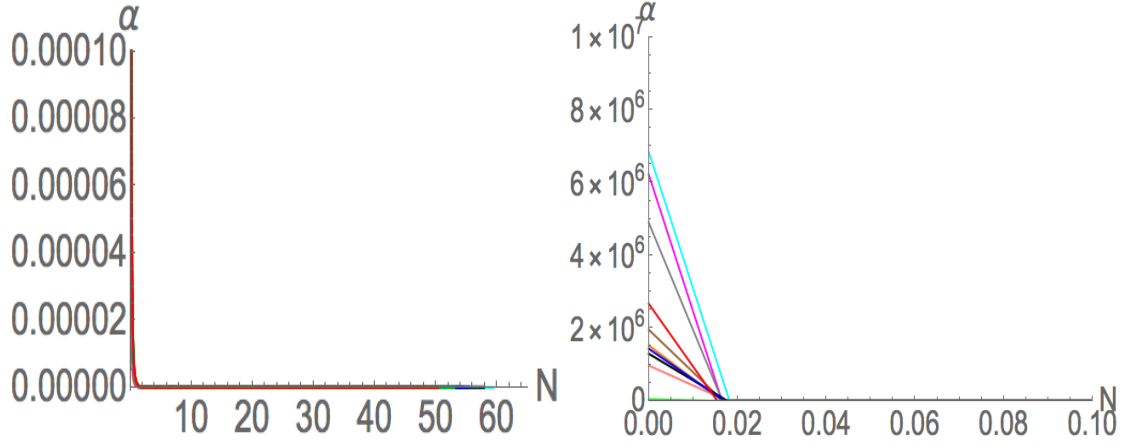


Figure 16: Left: Evolutions of the turn rate per Hubble parameter $\alpha(N) = 2\omega(N)/H(N)$. Right: A close shot of evolutions of $\alpha(N)$ for $\rho = 3$. Various colors refer to various parameter sets listed on Table 11.

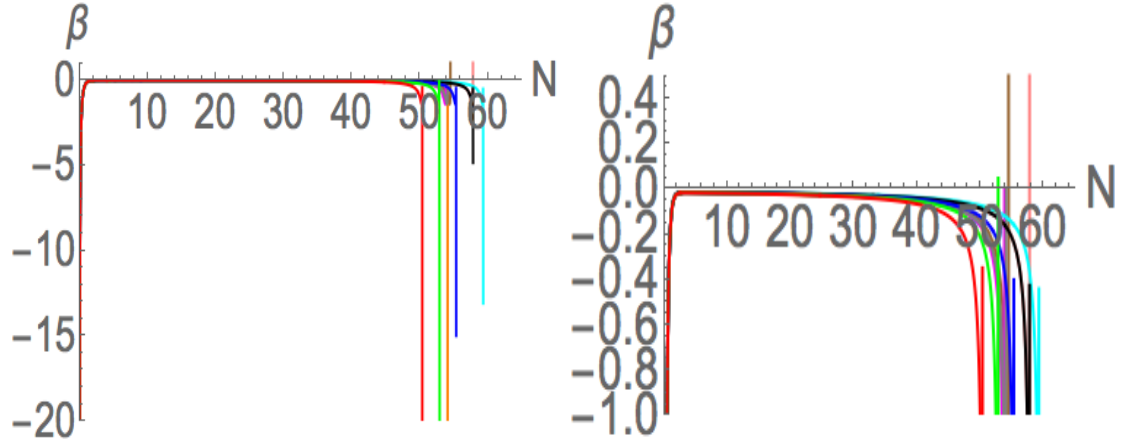


Figure 17: Left: Evolutions of $\beta(N)$. Right: A closed shot of evolutions of $\beta(N)$ for $\rho = 3$. Various colors refer to various parameter sets listed on Table 11.

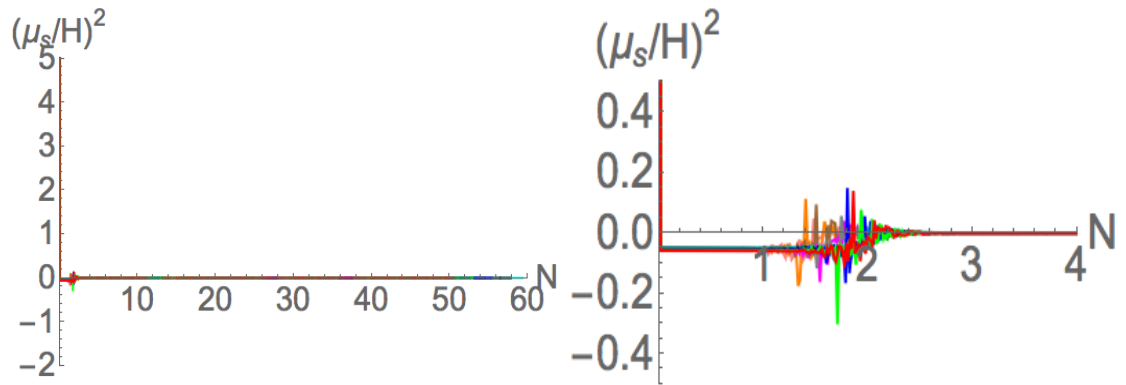


Figure 18: Left: Evolutions of $(\mu_s/H)^2$ for $\rho = 3$. Right: A close shot from 0 to 4 e-foldings. Various colors refer to various parameter sets listed on Table 11.

where $f(\phi^I)$ is the non-minimal coupling function and $\tilde{V}(\phi^I)$ is the potential for the scalar fields in the Jordan frame. To change the equation in Jordan frame into the counterpart in Einstein frame, we define a spacetime metric in the Einstein frame $g_{\mu\nu}(x)$ as

$$g_{\mu\nu}(x) = \Omega^2(x) \tilde{g}_{\mu\nu}(x), \quad (74)$$

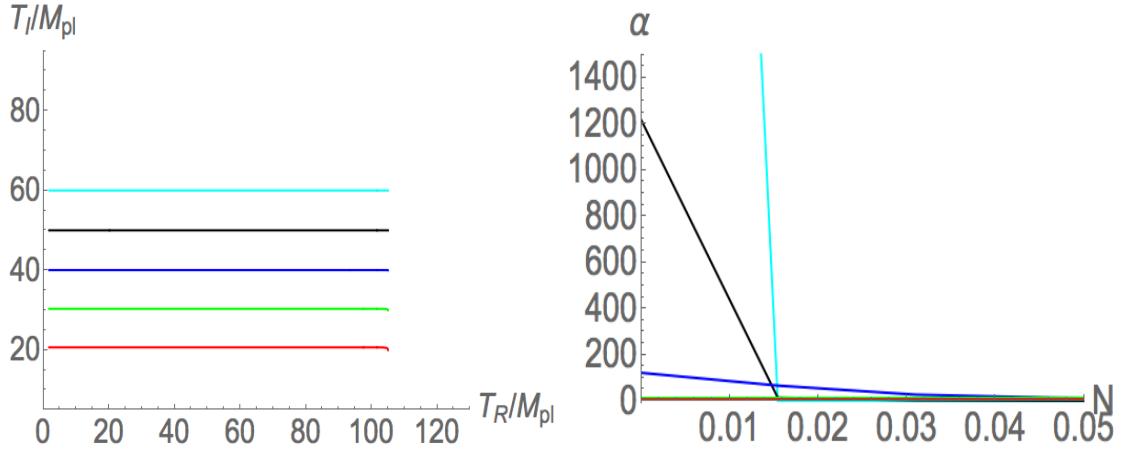


Figure 19: Field evolution at different α (N) (Left) and their corresponding initial turn rate per Hubble parameter (Right). Here, the field value T_I does not affect the strength of α (N). Thus, for obvious observation, we evaluate at different T_I . Various colors refer to various parameter sets listed on Table 12.

where the conformal factor $\Omega^2(x)$ is given by

$$\Omega^2(x) = \frac{2}{M_{\text{pl}}^2} f(\phi^I(x)). \quad (75)$$

Then, the action in Jordan frame becomes that in Einstein frame, which is given by

$$S_{\text{Einstein}} = \int d^4x \sqrt{-g} \left[\frac{M_{\text{pl}}^2}{2} R - \frac{1}{2} \mathcal{G}_{IJ} g^{\mu\nu} \nabla_\mu \phi^I \nabla_\nu \phi^J - V(\phi^I) \right]. \quad (76)$$

and the potential in the Einstein frame becomes

$$V(\phi^I) = \frac{\tilde{V}(\phi^I)}{\Omega^4(x)} = \frac{M_{\text{pl}}^4}{4f^2(\phi^I)} \tilde{V}(\phi^I). \quad (77)$$

The coefficients \mathcal{G}_{IJ} of the non-canonical kinetic terms in the Einstein frame depend on the non-minimal coupling function $f(\phi^I)$ and its derivatives. They are given by

$$\mathcal{G}_{IJ}(\phi^K) = \frac{M_{\text{pl}}^2}{2f(\phi^L)} \left[\tilde{\mathcal{G}}_{IJ}(\phi^K) + \frac{3}{f(\phi^L)} f_{,I} f_{,J} \right], \quad (78)$$

where $f_{,I} = \frac{\partial f}{\partial \phi^I}$. Varying the action in Einstein frame with respect to $g_{\mu\nu}(x)$, we have the Einstein equations

$$R_{\mu\nu} - \frac{1}{2} g_{\mu\nu} R = \frac{1}{M_{\text{pl}}^2} T_{\mu\nu}, \quad (79)$$

where

$$T_{\mu\nu} = \mathcal{G}_{IJ} \partial_\mu \phi^I \partial_\nu \phi^J - g_{\mu\nu} \left[\frac{1}{2} \mathcal{G}_{KL} \partial_\gamma \phi^K \partial^\gamma \phi^L + V(\phi^K) \right]. \quad (80)$$

Varying Eq. (77) with respect to ϕ^I , we obtain the equation of motion for ϕ^I

$$\square \phi^I + g^{\mu\nu} \Gamma_{JK}^I \partial_\mu \phi^J \partial_\nu \phi^K - \mathcal{G}^{IK} V_{,K} = 0, \quad (81)$$

where $\square \phi^I = g^{\mu\nu} \phi^I_{;\mu\nu}$ and Γ_{JK}^I is the Christoffel symbol for the field space manifold in terms of \mathcal{G}_{IJ} and its derivative. Expanding each scalar field to the first order around its classical background value,

$$\phi^I(x^\mu) = \varphi^I(t) + \delta \phi^I(x^\mu), \quad (82)$$

and perturbing a spatially flat Friedmann-Robertson-Walker (FRW) metric,

$$ds^2 = g_{\mu\nu} dx^\mu dx^\nu = -(1 + 2A) dt^2 + 2a (\partial_i B) dx^i dt + a^2 [(1 - 2\psi) \delta_{ij} + 2\partial_i \partial_j E] dx^i dx^j, \quad (83)$$

where $a(t)$ is the scale factor. To the zeroth order, the 00 and ij components of the Einstein equations become

$$H^2 = \frac{1}{3M_{\text{pl}}^2} \left[\frac{1}{2} \mathcal{G}_{IJ} \dot{\varphi}^I \dot{\varphi}^J + V(\varphi^I) \right], \quad (84)$$

$$\dot{H} = -\frac{1}{2M_{\text{pl}}^2} \mathcal{G}_{IJ} \dot{\varphi}^I \dot{\varphi}^J, \quad (85)$$

where $H = \frac{\dot{a}(t)}{a(t)}$ is the Hubble parameter, and the field field space metric is calculated at the zeroth order, $\mathcal{G}_{IJ} = \mathcal{G}_{IJ}(\varphi^K)$. Introducing the number of e-folding $N = \ln a$ with $dN = H dt$, the above Einstein equation becomes

$$3M_{\text{pl}}^2 - \frac{1}{2} \mathcal{G}_{IJ} \varphi^{I'} \varphi^{J'} = \frac{V(\varphi^I)}{H^2}, \quad (86)$$

$$\frac{H'}{H} = -\frac{1}{2M_{\text{pl}}^2} \mathcal{G}_{IJ} \varphi^{I'} \varphi^{J'}, \quad (87)$$

where the prime $'$ means the derivative with respect to N . For any vector in the field space A^I , we define a covariant derivative with respect to the field-space metric as usual by

$$\mathcal{D}_J A^I = \partial_J A^I + \Gamma_{JK}^I A^K, \quad (88)$$

and the time derivative with respect to the cosmic time t is given by

$$\mathcal{D}_t A^I \equiv \dot{\varphi}^J \mathcal{D}_J A^I = \dot{A}^I + \Gamma_{JK}^I \dot{\varphi}^J A^K = H \left(A^{I'} + \Gamma_{JK}^I \varphi^{J'} A^K \right). \quad (89)$$

Now, we define the length of the velocity vector for the background fields as

$$|\dot{\varphi}^I| \equiv \dot{\sigma} = \sqrt{\mathcal{G}_{PQ} \dot{\varphi}^P \dot{\varphi}^Q} \quad \Rightarrow \quad |\varphi^{I'}| \equiv \sigma' = \sqrt{\mathcal{G}_{PQ} \varphi^{P'} \varphi^{Q'}}. \quad (90)$$

Introducing the unit vector of the velocity vector of the background fields

$$\hat{\sigma}^I \equiv \frac{\dot{\varphi}^I}{\dot{\sigma}} = \frac{\varphi^{I'}}{\sigma'} = \frac{\varphi^{I'}}{\sqrt{\mathcal{G}_{PQ} \varphi^{P'} \varphi^{Q'}}} \quad (91)$$

the 00 and ij components of the Einstein equations become

$$H^2 = \frac{1}{3M_{\text{pl}}^2} \left[\frac{1}{2} \dot{\sigma}^2 + V \right] \quad \Leftrightarrow \quad 3M_{\text{pl}}^2 - \frac{1}{2} \sigma'^2 = \frac{V(\varphi^I)}{H^2} \quad \Leftrightarrow \quad \frac{V}{M_{\text{pl}}^2 H^2} = (3 - \epsilon), \quad (92)$$

$$\dot{H} = -\frac{1}{2M_{\text{pl}}^2} \dot{\sigma}^2 \quad \Leftrightarrow \quad \frac{H'}{H} = -\frac{1}{2M_{\text{pl}}^2} \sigma'^2 \quad \Leftrightarrow \quad \frac{\dot{\sigma}^2}{M_{\text{pl}}^2 H^2} = 2\epsilon, \quad (93)$$

and the equation of motion of ϕ^I in the zeroth order is

$$\ddot{\sigma} + 3H\dot{\sigma} + V_{,\sigma} = 0 \quad \Leftrightarrow \quad \frac{\ddot{\sigma}}{H\dot{\sigma}} = -3 - \frac{3 - \epsilon}{2\epsilon} \frac{d}{dN} (\ln V), \quad (94)$$

where

$$V_{,\sigma} \equiv \hat{\sigma}^I V_{,I}. \quad (95)$$

and ϵ is the first order Hubble slow-roll parameter defined in Eq.(98). Now, we define a quantity \hat{s}^{IJ} to obtain the field component orthogonal to $\hat{\sigma}^I$

$$\hat{s}^{IJ} \equiv \mathcal{G}^{IJ} - \hat{\sigma}^I \hat{\sigma}^J, \quad (96)$$

which obeys the following relations with $\hat{\sigma}^I$

$$\begin{aligned} \hat{\sigma}_I \hat{\sigma}^I &= 1, \\ \hat{s}^{IJ} \hat{s}_{IJ} &= \mathcal{N} - 1, \\ \hat{s}_A^I \hat{s}_J^A &= \hat{s}_J^I, \\ \hat{\sigma}_I \hat{s}^{IJ} &= 0 \quad \forall J. \end{aligned} \quad (97)$$

The slow-roll parameters are given by

$$\epsilon \equiv -\frac{\dot{H}}{H^2} = \frac{3\dot{\sigma}^2}{\dot{\sigma}^2 + 2V} \quad \Leftrightarrow \quad \frac{\dot{\sigma}^2}{V} = \frac{2\epsilon}{3 - \epsilon}, \quad (98)$$

and

$$\eta_{\sigma\sigma} \equiv M_{\text{pl}}^2 \frac{\mathcal{M}_{\sigma\sigma}}{V} \quad \text{and} \quad \eta_{ss} \equiv M_{\text{pl}}^2 \frac{\mathcal{M}_{ss}}{V}, \quad (99)$$

where \mathcal{M}_J^I is the effective mass squared matrix given by

$$\begin{aligned} \mathcal{M}_J^I &\equiv \mathcal{G}^{IK} (\mathcal{D}_J \mathcal{D}_K V) - \mathcal{R}_{LMJ}^I \dot{\phi}^L \dot{\phi}^M, \\ \mathcal{M}_{\sigma J} &\equiv \hat{\sigma}_I \mathcal{M}_J^I = \hat{\sigma}^K (\mathcal{D}_K \mathcal{D}_J V), \\ \mathcal{M}_{\sigma\sigma} &\equiv \hat{\sigma}_I \hat{\sigma}^J \mathcal{M}_J^I = \hat{\sigma}^K \hat{\sigma}^J (\mathcal{D}_K \mathcal{D}_J V), \\ \mathcal{M}_{sJ} &\equiv \hat{s}_I \mathcal{M}_J^I = \hat{s}_I (\mathcal{G}^{IK} (\mathcal{D}_J \mathcal{D}_K V) - \mathcal{R}_{LMJ}^I \dot{\phi}^L \dot{\phi}^M), \\ \mathcal{M}_{ss} &\equiv \hat{s}_I \hat{s}^J \mathcal{M}_J^I = \hat{s}_I \hat{s}^J (\mathcal{G}^{IK} (\mathcal{D}_J \mathcal{D}_K V) - \mathcal{R}_{LMJ}^I \dot{\phi}^L \dot{\phi}^M), \end{aligned} \quad (100)$$

and \hat{s}^I is defined in the following argument. Now we define the turn-rate vector ω^I as the covariant rate of change of the unit vector $\hat{\sigma}^I$

$$\omega^I \equiv \mathcal{D}_t \hat{\sigma}^I = -\frac{1}{\dot{\sigma}} V_{,K} \hat{s}^{IK} = \frac{-1}{H\dot{\sigma}} V_{,K} \hat{s}^{IK}. \quad (101)$$

Since $\omega^I \propto \hat{s}^{IK}$, we have

$$\omega^I \hat{\sigma}_I = 0. \quad (102)$$

We can also find

$$\mathcal{D}_t \hat{s}^{IJ} = -\hat{\sigma}^I \omega^J - \hat{\sigma}^J \omega^I. \quad (103)$$

Also, we introduce a new unit vector \hat{s}^I pointing in the direction of the turn-rate, ω^I , and a new projection operator γ^{IJ}

$$\hat{s}^I \equiv \frac{\omega^I}{\omega}, \quad (104)$$

$$\gamma^{IJ} \equiv \mathcal{G}^{IJ} - \hat{\sigma}^I \hat{\sigma}^J - \hat{s}^I \hat{s}^J. \quad (105)$$

where $\omega = |\omega^I|$ is the magnitude of the turn-rate vector. The new unit vector \hat{s}^I and the new projection operator γ^{IJ} also satisfy

$$\begin{aligned} \hat{s}^{IJ} &= \hat{s}^I \hat{s}^J + \gamma^{IJ}, \\ \gamma^{IJ} \gamma_{IJ} &= \mathcal{N} - 2, \\ \hat{s}^{IJ} \hat{s}_J &= \hat{s}^I, \\ \hat{\sigma}_I \hat{s}^I &= \hat{\sigma}_I \gamma^{IJ} = \hat{s}_I \gamma^{IJ} = 0 \quad \forall J. \end{aligned} \quad (106)$$

We then find

$$\mathcal{D}_t \hat{s}^I = -\omega \hat{\sigma}^I - \Pi^I, \mathcal{D}_t \gamma^{IJ} = \hat{s}^I \gamma^J + \hat{s}^J \gamma^I, \quad (107)$$

where

$$\Pi^I \equiv \frac{1}{\omega} \mathcal{M}_{\sigma K} \gamma^{IK}, \quad (108)$$

and hence

$$\hat{\sigma}_I \Pi^I = \hat{s}_I \Pi^I = 0, \quad (109)$$

Now, we define the curvature and entropic perturbations as follows

$$\mathcal{R} = \psi + \frac{H}{\dot{\sigma}} \hat{\sigma}_J \delta \phi^J = \frac{H}{\dot{\sigma}} Q_\sigma, \quad (110)$$

$$\mathcal{S} = \frac{H}{\dot{\sigma}} Q_s, \quad (111)$$

whose E.O.M.s are given by [9]

$$\begin{aligned} \ddot{Q}_\sigma + 3H\dot{Q}_\sigma + \left[\left(\frac{k}{a} \right)^2 + \mathcal{M}_{\sigma\sigma} - \omega^2 - \frac{1}{M_{\text{pl}}^2 a^3} \frac{d}{dt} \left(\frac{a^3 \dot{\sigma}^2}{H} \right) \right] Q_\sigma &= 2 \frac{d}{dt} (\omega Q_s) - 2 \left(\frac{V_{,\sigma}}{\dot{\sigma}} + \frac{\dot{H}}{H} \right) \omega Q_s, \\ \ddot{Q}_s + 3H\dot{Q}_s + \left[\left(\frac{k}{a} \right)^2 + \mathcal{M}_{ss} + 3\omega^2 \right] Q_s &= 4M_{\text{pl}}^2 \frac{\omega}{\dot{\sigma}} \frac{k^2}{a^2} \Psi, \end{aligned} \quad (112)$$

where Ψ is the gauge-invariant Bardeen potential [7, 8], $\mathcal{M}_{\sigma\sigma}$ and \mathcal{M}_{ss} are given by Eq.(100) and

$$\mu_s^2 = \mathcal{M}_{ss} + 3\omega^2, \quad (113)$$

is an effective square mass of entropy perturbations. After the first horizon crossing, the co-moving wave number k obeys $\frac{k}{aH} < 1$. Hence, the curvature and entropic perturbations satisfy the following equations

$$\dot{\mathcal{R}} = \alpha H \mathcal{S} + O\left(\frac{k^2}{a^2 H^2}\right), \quad (114)$$

$$\dot{\mathcal{S}} = \beta H \mathcal{S} + O\left(\frac{k^2}{a^2 H^2}\right), \quad (115)$$

which allows us to write the transfer functions

$$T_{\mathcal{RS}}(t_{\text{hc}}, t) = \int_{t_{\text{hc}}}^t dt' \alpha(t') H(t') T_{\mathcal{SS}}(t_{\text{hc}}, t'), \quad (116)$$

$$T_{\mathcal{SS}}(t_{\text{hc}}, t) = \exp \left[\int_{t_{\text{hc}}}^t dt' \beta(t') H(t') \right]. \quad (117)$$

where t_{hc} is the time of the first horizon crossing. Being changed from the cosmic time t into the number of e-folding $N = \ln a$, where $dN = H dt$ ⁷, $T_{\mathcal{RS}}(t_{\text{hc}}, t)$ and $T_{\mathcal{SS}}(t_{\text{hc}}, t)$ become

$$T_{\mathcal{RS}}(N_{\text{hc}}, N) = \int_{N_{\text{hc}}}^N dN' \alpha(N') T_{\mathcal{SS}}(N_{\text{hc}}, N'), \quad (118)$$

⁷In some literatures like [9], $N_* = N_{\text{tot}} - N(t)$ is used and the corresponding differential equation becomes $dN_* = -H dt$. But, in this paper, we keep using $dN = H dt$.

and

$$T_{SS}(N_{\text{hc}}, N) = \exp \left[\int_{N_{\text{hc}}}^N dN' \beta(N') \right]. \quad (119)$$

Now that the E.O.M.s of curvature and entropic perturbations are [6]

$$\dot{\mathcal{R}} = 2\omega\mathcal{S} + O\left(\frac{k^2}{a^2 H^2}\right), \quad (120)$$

and

$$\dot{Q}_s \simeq -\frac{\mu_s^2}{3H} Q_s, \quad (121)$$

where the effective squared mass of the entropy perturbation can be written as that relative to the Hubble scale as

$$\mu_s^2 = \mathcal{M}_{ss} + 3\omega^2 \quad \Leftrightarrow \quad \frac{\mu_s^2}{H^2} = (3 - \epsilon) \eta_{ss} + \frac{3}{4} \alpha^2, \quad (122)$$

and \simeq means slow-roll approximation and α is given in Eq.(123). Comparing with Eq.(110), (111), (114) and (115) with Eq.(120) and (121) [6], we obtain

$$\alpha(t) = \frac{2\omega(t)}{H(t)} \quad \Leftrightarrow \quad \alpha(N) = \frac{2\omega(N)}{H(N)}, \quad (123)$$

and

$$\beta = -\frac{\mu_s^2}{3H^2} - \epsilon - \frac{\ddot{\sigma}}{H\dot{\sigma}} = -\eta_{ss} \left(1 - \frac{1}{3}\epsilon\right) + (3 - \epsilon) + \frac{3 - \epsilon}{2\epsilon} \frac{d}{dN} (\ln V) - \frac{1}{4} \alpha^2, \quad (124)$$

Note that the power spectrum for the gauge invariant curvature perturbation is given by

$$\langle \mathcal{R}(\mathbf{k}_1) \mathcal{R}(\mathbf{k}_2) \rangle = (2\pi)^3 \delta^{(3)}(\mathbf{k}_1 + \mathbf{k}_2) P_{\mathcal{R}}(k_1), \quad (125)$$

where $P_{\mathcal{R}}(k) = |\mathcal{R}|^2$. The dimensionless power spectrum is

$$\mathcal{P}_{\mathcal{R}} = \frac{k^3}{2\pi^2} |\mathcal{R}|^2, \quad (126)$$

and the spectral index is defined as

$$n_s \equiv 1 + \frac{d \ln \mathcal{P}_{\mathcal{R}}}{d \ln k_{\text{hc}}}, \quad (127)$$

where $k_{\text{hc}} = a(t_{\text{hc}}) H(t_{\text{hc}})$ represents the pivot scale at the first horizon crossing t_{hc} , which is related to the cosmic time t by

$$\frac{d \ln k}{dt} = \frac{d(aH)}{dt} = \frac{\dot{a}}{a} + \frac{\dot{H}}{H} = H \left(1 + \frac{\dot{H}}{H^2}\right) = (1 - \epsilon) H. \quad (128)$$

Using the transfer function, we can relate the power spectra of adiabatic and entropic perturbations at time t_{hc} to its value at some later time $t > t_{\text{hc}}$ with the corresponding pivot scale k as

$$\begin{aligned} \mathcal{P}_{\mathcal{R}}(k) &= \mathcal{P}_{\mathcal{R}}(k_{\text{hc}}) [1 + T_{\mathcal{RS}}^2(t_{\text{hc}}, t)], \\ \mathcal{P}_{\mathcal{S}}(k) &= \mathcal{P}_{\mathcal{R}}(k_{\text{hc}}) T_{\mathcal{SS}}^2(t_{\text{hc}}, t), \end{aligned} \quad (129)$$

The transfer functions are given by

$$\begin{aligned}\frac{1}{H(t_{\text{hc}})} \frac{\partial T_{\mathcal{RS}}(t_{\text{hc}}, t)}{\partial t_{\text{hc}}} &= -\alpha(t_{\text{hc}}) - \beta(t_{\text{hc}}) T_{\mathcal{SS}}(t_{\text{hc}}, t), \\ \frac{1}{H(t_{\text{hc}})} \frac{\partial T_{\mathcal{SS}}(t_{\text{hc}}, t)}{\partial t_{\text{hc}}} &= -\beta(t_{\text{hc}}) T_{\mathcal{SS}}(t_{\text{hc}}, t).\end{aligned}\tag{130}$$

In term of the number of e-folding N , the above differential equation becomes

$$\begin{aligned}\frac{\partial T_{\mathcal{RS}}(N_{\text{hc}}, N)}{\partial N_{\text{hc}}} &= -\alpha(N_{\text{hc}}) - \beta(N_{\text{hc}}) T_{\mathcal{SS}}(N_{\text{hc}}, N), \\ \frac{\partial T_{\mathcal{SS}}(N_{\text{hc}}, N)}{\partial N_{\text{hc}}} &= -\beta(N_{\text{hc}}) T_{\mathcal{SS}}(N_{\text{hc}}, N).\end{aligned}\tag{131}$$

The spectral index for the power spectrum of the adiabatic fluctuations becomes

$$n_s \simeq n_s(t_{\text{hc}}) + \frac{1}{H} \left(\frac{\partial T_{\mathcal{RS}}}{\partial t_{\text{hc}}} \right) \sin 2\Delta,\tag{132}$$

where

$$n_s(t_{\text{hc}}) = 1 - 6\epsilon(t_{\text{hc}}) + 2\eta_{\sigma\sigma}(t_{\text{hc}}),\tag{133}$$

and the trigonometric functions for $T_{\mathcal{RS}}$ are defined as

$$\sin \Delta \equiv \frac{1}{\sqrt{1 + T_{\mathcal{RS}}^2}}, \quad \cos \Delta \equiv \frac{T_{\mathcal{RS}}}{\sqrt{1 + T_{\mathcal{RS}}^2}}, \quad \tan \Delta \equiv \frac{1}{T_{\mathcal{RS}}}.\tag{134}$$

The iso-curvature fraction is given by

$$\beta_{\text{iso}} \equiv \frac{\mathcal{P}_{\mathcal{S}}}{\mathcal{P}_{\mathcal{R}} + \mathcal{P}_{\mathcal{S}}} = \frac{T_{\mathcal{SS}}^2}{1 + T_{\mathcal{SS}}^2 + T_{\mathcal{RS}}^2},\tag{135}$$

which can be used for compared with the recent observables in Planck collaboration. Also, the tensor-to-scalar ratio is given by

$$r \simeq \frac{16\epsilon}{1 + T_{\mathcal{RS}}^2}.\tag{136}$$

References

- [1] Alan H. Guth, *Inflationary universe: A possible solution to the horizon and flatness problems*, Phys. Rev. D23 (1981), 347-356
- [2] A. A. Starobinsky, *A new type of isotropic cosmological models without singularity*, Phys. Lett. B91 (1980), 99-102
- [3] K. Sato, *First-order phase transition of a vacuum and the expansion of the Universe*, Mon. Not. Roy. Astron. Soc. 195 (1981), 467-479
- [4] Jerome Martin, Christophe Ringeval, Vincent Vennin, *Encyclopaedia Inflationaris*, Phys.Dark Univ. 5-6 (2014), 75-235, arXiv: 1303.3787
- [5] Planck Collaboration, *Planck 2018 results. X. Constraints on inflation*, 2018, arXiv: 1807.06211

- [6] David I. Kaiser, Edward A. Mazenc, and Evangelos I. Sfakianakis, *Primordial bispectrum from multifield inflation with nonminimal couplings*, Physical Review D 87, 064004 (2013), arXiv: 1210.7487
- [7] Bruce A. Bassett, Shinji Tsujikawa, and David Wands, *Inflation dynamics and reheating*, Review of Modern Physics 78 (2006) 537, arXiv: astro-ph/0507632
- [8] Karim A. Malik, David Wands, *Cosmological perturbations*, Physics Reports Volume 475, Issues 1-4, 2009, pages 1-51, arXiv: 0809.4944
- [9] Katelin Schutz, Evangelos I. Sfakianakis, David I. Kaiser, *Multifield inflation after Planck: iso-curvature modes from non-minimal couplings*, Physical Review D 89, 064044 (2014), arXiv: 1310.8285
- [10] L. Sebastiani, G. Cognola, R. Myrzakulov, S.D. Odintsov, S. Zerbini, *Nearly Starobinsky inflation from modified gravity*, Phys. Rev. D 89, 023518 (2014), arXiv: 1311.0744
- [11] S.D. Odintsov, V.K. Oikonomou, *Singular deformations of nearly R^2 inflation potentials*, Classical and Quantum Gravity 32 (2015) 235011, arXiv: 1504.01772
- [12] L. Sebastiani, G. Cognola, R. Myrzakulov, S.D. Odintsov, S. Zerbini, *Spotting deviations from R^2 inflation*, JCAP 05 (2016) 060, arXiv:1603.05537
- [13] S. Nojiri, S.D. Odintsov, V.K. Oikonomou, *Modified Gravity Theories on a Nutshell: Inflation, Bounce and Late-time Evolution*, Phys.Rept. 692 (2017) 1-104, arXiv: 1705.11098
- [14] S.D. Odintsov, V.K. Oikonomou, L. Sebastiani, *Unification of Constant-roll Inflation and Dark Energy with Logarithmic R^2 -corrected and Exponential $F(R)$ Gravity*, Nucl. Phys. B Vol. 923 (2017) 608-632, arXiv: 1708.08346
- [15] M. Kawasaki, Masahide Yamaguchi, T. Yanagida, *Natural chaotic inflation in supergravity*, Phys. Rev. Lett. 85 (2000), 3572-3575, arXiv: hep-ph/0004243
- [16] Renata Kallosh, Andrei Linde, Tomas Rube, *General inflaton potentials in supergravity*, Phys. Rev. D 83 (2011), 043507, arXiv: 1011.5945
- [17] Sergio Ferrara, Renata Kallosh, Andrei Linde, Massimo Porrati, *Minimal supergravity models of inflation*, Phys. Rev. D 88 (2013), 085038, arXiv: 1307.7696
- [18] Fotis Farakos, Rikard von Unge, *Naturalness and chaotic inflation in supergravity models of inflation*, JHEP 08(2014)168, arXiv: 1404.3739
- [19] F. Farakos, A. Kehagias, A. Riotto, *On the Starobinsky Model of Inflation from Supergravity*, Nuclear Physics B 876 (2013) 187-200, arXiv: 1307.1137
- [20] Sergio Ferrara, Renata Kallosh, Andrei Linde and Massimo Porrati, *Higher order corrections in minimal supergravity models of inflation*, JCAP 11 (2013) 046, arXiv: 1309.1085
- [21] I. Antoniadis, A. Chatrabhuti, H. Isono, R. Kneops, *Inflation from Supergravity with Gauged R -symmetry in de Sitter Vacuum*, Eur. Phys. J. C (2016) 76:680, arXiv: 1608.02121
- [22] Niccol  Cribiori, Fotis Farakos, Magnus Tournoy, and Antoine Van Proeyen, *Fayet-Iliopoulos terms in supergravity without gauged R -symmetry*, JHEP 04 (2018) 032, arXiv: 1712.08601

- [23] Sergei M. Kuzenko, *Taking a vector supermultiplet apart: Alternative Fayet-Iliopoulos-type terms*, Physics Letters B 781 (2018) 723-727, arXiv: 1801.04794
- [24] Yermek Aldabergenov, Auttakit Chatrabhuti, Sergei V. Ketov, *Generalized dilaton-axion models of inflation, de Sitter vacua and spontaneous SUSY breaking in supergravity*, Eur. Phys. J. C (2019) 79: 713, arXiv: 1907.10373
- [25] John R. Ellis, C. Kounnas, Dimitri V. Nanopoulos, *Phenomenological $SU(1,1)$ supergravity*, Nuclear Physics B 241 (1984) 406-428
- [26] John Ellis, Marcos A.G. Garcia, Dimitri V. Nanopoulos and Keith A. Olive, *Phenomenological aspects of no-scale inflation models*, JCAP 1510 (10) 003, 2015, arXiv: 1503.08867
- [27] John Ellis, Marcos A. G. Garcia, Dimitri V. Nanopoulos, Keith A. Olive, *No-scale inflation*, Classical and Quantum Gravity, 33(9), 094001 (2016), arXiv: 1507.02308
- [28] John Ellis, Dimitri V. Nanopoulos, Keith A. Olive, *From R^2 gravity to no-scale supergravity*, Physical Review D 97, 043530 (2018), arXiv: 1711.11051
- [29] John Ellis, Balakrishnan Nagaraj, Dimitri V. Nanopoulos, Keith A. Olive, *De Sitter vacua in no-scale supergravity*, JHEP 11 (2018) 110, arXiv: 1809.10114
- [30] John Ellis, Dimitri V. Nanopoulos, Keith A. Olive, Sarunas Verner, *A general classification of Starobinsky like inflationary avatars of $SU(2,1)/SU(2) \times U(1)$ No-Scale Supergravity*, JHEP 03 (2019) 099, arXiv: 1812.02192
- [31] John Ellis, Dimitri V. Nanopoulos, Keith A. Olive and Sarunas Verner, *Unified no-scale attractors*, JCAP 09 (2019) 040, arXiv: 1906.10176
- [32] M. J. Duff, S. Ferrara, *Generalized mirror symmetry and trace anomalies*, Classical and Quantum Gravity 28 065005 (2011), arXiv: 1009.4439
- [33] M. J. Duff, S. Ferrara, *Four curious supergravities*, Physical Review D 83, 046007 (2011), arXiv: 1010.3173
- [34] Sergio Ferrara, Renata Kallosh, *Seven-Disk Manifold, alpha-attractors and B-modes*, Physical Review D 94, 126015 (2016), arXiv: 1610.04163
- [35] Calcagni, Gianluca, *Classical and Quantum Cosmology*, Graduate Texts in Physics, Springer, 2017

Color	ι_1	ι_2/ι_1	$M_{3/2-}/M_{\text{pl}}$	$F_T _-/M_{\text{pl}}$	T_{Rend}	T_{Iend}	T_{Rhic}	T_{Thc}	N_{end}	N_{stop}	β_{iso}	$\cos(\Delta)$
Gray	25	-5	1.2×10^{-4}	6.912×10^{-5}	6.25	62.5	68	83	50.4485	53.8960	1.87873×10^{-39}	2.2983×10^{-5}
Magenta	27	-8	1.1111×10^{-4}	5.9259×10^{-5}	6.75	108	70	145	59.3514	63.2240	5.48281×10^{-40}	2.86372×10^{-5}
Brown	28	-6	1.0714×10^{-4}	5.5102×10^{-5}	7	84	73	120	57.3194	61.1881	5.32875×10^{-39}	2.58454×10^{-5}
Orange	29	-5	1.0344×10^{-4}	5.1367×10^{-5}	7.25	72.5	77	110	59.1943	63.0620	6.85479×10^{-38}	2.52503×10^{-5}
Pink	30	-4.5	5×10^{-4}	4.8×10^{-5}	7.5	67.5	81	100	55.2191	59.0726	1.11729×10^{-39}	2.15684×10^{-5}
Red	34	-6	4.41176×10^{-4}	3.73702×10^{-5}	8.5	102	88	145	56.0756	59.9293	5.14412×10^{-37}	2.08999×10^{-5}
Green	34	-6	4.41176×10^{-4}	3.73702×10^{-5}	8.5	102	92	140	56.2624	59.9871	1.35243×10^{-42}	1.94259×10^{-5}
Blue	34	-6	4.41176×10^{-4}	3.73702×10^{-5}	8.5	102	84	149	55.6707	59.5427	4.45289×10^{-40}	2.29009×10^{-5}
Black	34	-6	4.41176×10^{-4}	3.73702×10^{-5}	8.5	102	79	156	57.9958	61.0403	4.68586×10^{-43}	3.08396×10^{-5}
Cyan	34	-6	4.41176×10^{-4}	3.73702×10^{-5}	8.5	102	75	160	58.9596	62.0001	2.30095×10^{-41}	4.50112×10^{-5}

Table 5: Feasible parameter sets for inflation for $\omega_1 > 0$ (or $\iota_1 > 0$) and $\rho = 4$. Recall the unit of each variable is the following. $[\iota_1] = M_{\text{pl}}$, $[M_{3/2-}] = M_{\text{pl}}$, $[F_T|_-] = M_{\text{pl}}^2$, $[T_{\text{Rend}}] = [T_{\text{Iend}}] = [T_{\text{Rhic}}] = [T_{\text{Thc}}] = M_{\text{pl}}$. N_{end} is the e-folding number when $\epsilon = 1$, which represents the end of inflation. N_{stop} means the e-folding number that we stop the numerical calculation.

Color	ι_1	ι_2/ι_1	$M_{3/2-}/10^{-5}M_{\text{pl}}$	$F_T _-/10^{-5}M_{\text{pl}}^2$	T_{Rend}	T_{Iend}	T_{Rhic}	T_{Thc}	N_{end}	N_{stop}	β_{iso}	$\cos(\Delta)$
Gray	10	-5	19.7028	2.47431	8.3333	25	52	52	52.3575	55.9694	2.66698×10^{-36}	5.87517×10^{-5}
Magenta	12	-8.5	14.9884	1.56856	10	51	70	75	53.4696	57.5777	2.34071×10^{-38}	7.95594×10^{-5}
Brown	13	-7.5	13.2927	1.28409	10.8333	48.75	75	76	53.4769	57.4120	3.60886×10^{-38}	9.36358×10^{-5}
Orange	14	-6.5	11.8942	1.0669	11.6667	45.5	77	81	55.1485	59.2092	1.17279×10^{-37}	1.31272×10^{-4}
Pink	15	-5.5	10.7249	0.897895	12.5	41.25	77	83	52.765	56.8757	4.02109×10^{-35}	3.01275×10^{-5}
Red	16	-6	9.73528	0.764106	13.3333	48	82	93	53.206	57.3168	2.04007×10^{-36}	2.65296×10^{-5}
Green	16	-6	9.73528	0.764106	13.3333	48	86	88	51.9849	55.8550	5.58572×10^{-37}	9.72256×10^{-5}
Blue	16	-6	9.73528	0.764106	13.3333	48	90	85	53.8209	57.6154	2.09012×10^{-38}	2.90824×10^{-4}
Black	16	-6	9.73528	0.764106	13.3333	48	94	81	55.2881	58.4560	7.36786×10^{-37}	6.65673×10^{-5}
Cyan	16	-6	9.73528	0.764106	13.3333	48	92	86	57.56	61.5649	2.27647×10^{-39}	3.40788×10^{-4}

Table 6: Feasible parameter sets for inflation for $\omega_1 > 0$ (or $\iota_1 > 0$) and $\rho = 5$. Recall the unit of each variable is the following. $[\iota_1] = M_{\text{pl}}$, $[M_{3/2-}] = M_{\text{pl}}$, $[F_T|_-] = M_{\text{pl}}^2$, $[T_{\text{Rend}}] = [T_{\text{Iend}}] = [T_{\text{Rhic}}] = [T_{\text{Thc}}] = M_{\text{pl}}$. N_{end} is the e-folding number when $\epsilon = 1$, which represents the end of inflation. N_{stop} means the e-folding number that we stop the numerical calculation.

Color	ι_1	ι_2/ι_1	$M_{3/2-}/10^{-5}M_{\text{pl}}$	$F_T _-/10^{-5}M_{\text{pl}}^2$	T_{Rend}	T_{Ihc}	T_{Rhc}	T_{Ihc}	N_{end}	N_{stop}	β_{iso}	$\cos(\Delta)$
Gray	3	-5	5.0114	0.3251	13.5	7.5	66	30	52.2627	54.3395	2.39368×10^{-37}	8.4469×10^{-6}
Magenta	4	-6	2.81893	0.1372	18	12	92	40	56.1668	58.2761	6.7651×10^{-37}	9.20973×10^{-6}
Brown	5	-7	1.8041	0.07023	22.5	17.5	118	50	57.7282	59.8035	5.1486×10^{-38}	9.9622×10^{-6}
Orange	6	-8	1.2529	0.04064	27	24	142	60	55.6072	57.7068	5.51104×10^{-39}	1.01895×10^{-5}
Pink	7	-9	0.920467	0.0255952	31.5	31.5	170	70	57.8876	59.9947	3.22952×10^{-40}	1.2694×10^{-5}
Red	9	-10	0.556826	0.0120427	40.5	45	214	101	57.5722	59.6827	2.29669×10^{-41}	6.38619×10^{-6}
Green	9	-10	0.556826	0.0120427	40.5	45	210	105	56.6762	58.7541	4.01603×10^{-37}	4.91618×10^{-6}
Blue	9	-10	0.556826	0.0120427	40.5	45	206	110	56.6968	58.8117	7.46009×10^{-38}	3.73375×10^{-6}
Black	9	-10	0.556826	0.0120427	40.5	45	202	115	57.0605	59.1691	3.21796×10^{-39}	2.89628×10^{-6}
Cyan	9	-10	0.556826	0.0120427	40.5	45	199	118	56.9827	59.0902	5.66193×10^{-39}	2.46863×10^{-6}

Table 7: Feasible parameter sets for inflation for $\omega_1 > 0$ (or $\iota_1 > 0$) and $\rho = 6$. Recall the unit of each variable is the following. $[\iota_1] = M_{\text{pl}}$, $[M_{3/2-}] = M_{\text{pl}}$, $[F_T|_-] = M_{\text{pl}}^2$, $[T_{\text{Rend}}] = [T_{\text{Ihc}}] = [T_{\text{Rhc}}] = M_{\text{pl}}$. N_{end} is the e-folding number when $\epsilon = 1$, which represents the end of inflation. N_{stop} means the e-folding number that we stop the numerical calculation.

Color	ι_1	ι_2/ι_1	$M_{3/2+}/10^{-6}M_{\text{pl}}$	T_{Rend}	T_{Ihc}	T_{Rhc}	T_{Ihc}	N_{end}	N_{stop}	β_{iso}	$\cos(\Delta)$
Red	-14	11	2.67857	14	77	185	180	58.3165	62.6594	9.9157×10^{-40}	1.31875×10^{-5}
Green	-14	11	2.67857	14	77	190	175	58.1038	62.4462	4.82523×10^{-39}	1.14167×10^{-5}
Blue	-14	11	2.67857	14	77	195	170	58.0405	61.3501	3.07253×10^{-40}	1.02649×10^{-5}
Black	-14	11	2.67857	14	77	200	165	58.1267	61.4364	1.49867×10^{-40}	9.46949×10^{-6}
Cyan	-14	11	2.67857	14	77	205	160	58.3628	61.6725	6.49472×10^{-38}	8.89825×10^{-6}
Gray	-15	10	2.5	150	75	220	160	57.2553	60.5650	7.23189×10^{-35}	7.98833×10^{-6}
Magenta	-16	9	2.34375	144	72	233	160	55.8962	59.2060	2.04449×10^{-35}	7.30653×10^{-6}
Brown	-17	8	2.20588	136	68	250	160	56.3214	59.6312	2.21076×10^{-39}	6.80653×10^{-6}
Orange	-18	7	2.08333	126	63	265	160	56.3138	59.6237	3.33083×10^{-36}	6.41033×10^{-6}
Pink	-19	6	1.97368	114	57	280	160	56.5409	59.8508	4.60472×10^{-36}	6.10035×10^{-6}

Table 8: Feasible parameter sets for inflation for $\omega_1 < 0$ (or $\iota_1 < 0$) and $\rho = 4$. Note that the F term SUSY breaking scale is 0 for all real values of parameters and fields. Recall the unit of each variable is the following. $[\iota_1] = M_{\text{pl}}$, $[M_{3/2+}] = M_{\text{pl}}$, $[T_{\text{Rend}}] = [T_{\text{Ihc}}] = [T_{\text{Rhc}}] = [T_{\text{Ihc}}] = M_{\text{pl}}$. N_{end} is the e-folding number when $\epsilon = 1$, which represents the end of inflation. N_{stop} means the e-folding number that we stop the numerical calculation.

Color	ι_1	ι_2/ι_1	$M_{3/2+}/10^{-7}M_{\text{pl}}$	T_{Rend}	T_{Iend}	T_{Rhic}	T_{Ihc}	N_{end}	N_{stop}	β_{iso}	$\cos(\Delta)$
Red	-17	7	3.97837	14.1667	59.5	104	90	57.1196	61.1125	3.38902×10^{-38}	4.03578×10^{-5}
Green	-17	7	3.97837	14.1667	59.5	85	108	51.7453	54.9271	3.61843×10^{-37}	1.98477×10^{-5}
Blue	-17	7	3.97837	14.1667	59.5	90	107	56.0768	59.6890	8.03244×10^{-37}	3.27246×10^{-5}
Black	-17	7	3.97837	14.1667	59.5	100	98	58.6238	62.3304	7.06245×10^{-41}	1.10696×10^{-4}
Cyan	-17	7	3.97837	14.1667	59.5	95	103	57.4204	60.9148	1.34988×10^{-37}	1.23669×10^{-4}
Gray	-19	6	3.36704	95	57	110	98	54.8516	58.5579	3.8036×10^{-39}	7.51476×10^{-5}
Magenta	-21	5	2.89767	87.5	52.5	121	102	57.5109	61.5113	7.10984×10^{-38}	2.02087×10^{-4}
Brown	-23	4	2.52805	76.6667	46	128	106	57.8894	61.9445	2.08549×10^{-37}	6.69631×10^{-5}
Orange	-27	5	1.98762	112.5	67.5	160	115	52.3259	56.1155	6.41039×10^{-37}	2.44855×10^{-5}
Pink	-29	6	1.78559	145	87	160	160	55.1624	59.2207	3.48978×10^{-36}	7.42136×10^{-5}

Table 9: Feasible parameter sets for inflation for $\omega_1 < 0$ (or $\iota_1 < 0$) and $\rho = 5$. Note that the F term SUSY breaking scale is 0 for all real values of parameters and fields. Recall the unit of each variable is the following. $[\iota_1] = M_{\text{pl}}$, $[M_{3/2+}] = M_{\text{pl}}$, $[T_{\text{Rend}}] = [T_{\text{Iend}}] = [T_{\text{Rhic}}] = [T_{\text{Ihc}}] = M_{\text{pl}}$. N_{end} is the e-folding number when $\epsilon = 1$, which represents the end of inflation. N_{stop} means the e-folding number that we stop the numerical calculation.

Color	ι_1	ι_2/ι_1	$M_{3/2+}/10^{-8}M_{\text{pl}}$	T_{Rend}	T_{Iend}	T_{Rhic}	T_{Ihc}	N_{end}	N_{stop}	β_{iso}	$\cos(\Delta)$
Gray	-18	9	6.85871	121.5	81	60	100	58.2101	61.6281	8.06083×10^{-35}	6.77743×10^{-5}
Magenta	-20	8	5.55556	120	80	67	100	56.9523	60.5887	7.4834×10^{-35}	8.14647×10^{-5}
Brown	-22	7	4.59137	115.5	77	70	105	59.5551	63.1895	2.44999×10^{-35}	1.01176×10^{-5}
Orange	-24	6	3.85802	108	72	70	105	50.9481	54.7494	2.71462×10^{-35}	1.01176×10^{-5}
Pink	-26	6	3.28731	117	78	87	106	59.907	63.3246	5.44139×10^{-37}	4.42432×10^{-5}
Red	-30	5	2.46914	22.5	75	101	103	55.4472	58.8651	4.7257×10^{-37}	8.54936×10^{-5}
Green	-30	5	2.46914	22.5	75	100	107	58.682	62.0998	3.2964×10^{-37}	3.88947×10^{-5}
Blue	-30	5	2.46914	22.5	75	98	110	59.2057	62.8400	1.28312×10^{-34}	2.44867×10^{-5}
Black	-30	5	2.46914	22.5	75	95	113	58.3676	62.0021	1.44804×10^{-36}	1.58228×10^{-5}
Cyan	-30	5	2.46914	22.5	75	89	116	52.9635	56.7473	1.58416×10^{-34}	9.00233×10^{-6}

Table 10: Feasible parameter sets for inflation for $\omega_1 < 0$ (or $\iota_1 < 0$) and $\rho = 6$. Note that the F term SUSY breaking scale is 0 for all real values of parameters and fields. Recall the unit of each variable is the following. $[\iota_1] = M_{\text{pl}}$, $[M_{3/2+}] = M_{\text{pl}}$, $[T_{\text{Rend}}] = [T_{\text{Iend}}] = [T_{\text{Rhic}}] = [T_{\text{Ihc}}] = M_{\text{pl}}$. N_{end} is the e-folding number when $\epsilon = 1$, which represents the end of inflation. N_{stop} means the e-folding number that we stop the numerical calculation.

Color	$ \mu /M_{\text{pl}}^2$	ν_1/M_{pl}	$M_{3/2+}/M_{\text{pl}}$	$T_{\text{Rend}}/M_{\text{pl}}$	$T_{\text{Rhc}}/M_{\text{pl}}$	$T_{\text{Ihc}}/M_{\text{pl}}$	N_{end}	N_{stop}	β_{iso}	$\cos(\Delta)$
Gray	10^{-4}	-2	1.36083×10^{-5}	3	225	80	53.7825	54.1041	7.54744×10^{-36}	3.28888×10^{-6}
Magenta	10^{-4}	-2.5	1.21716×10^{-5}	3.75	280	80	53.5343	53.8559	1.36149×10^{-34}	2.63095×10^{-5}
Brown	10^{-4}	-3	1.11111×10^{-5}	4.5	340	80	54.1961	54.5177	1.68237×10^{-37}	2.19281×10^{-6}
Orange	10^{-4}	-4	9.6225×10^{-6}	6	450	80	53.7825	54.1041	2.19583×10^{-35}	1.64444×10^{-6}
Pink	10^{-4}	-5	8.60663×10^{-6}	7.5	600	80	57.5058	57.8274	7.62281×10^{-36}	1.31667×10^{-6}
Red	10^{-4}	-1	1.9245×10^{-5}	1.5	105	20	50.061	50.3826	7.23759×10^{-34}	6.57141×10^{-6}
Green	10^{-4}	-1	1.9245×10^{-5}	1.5	110	20	52.5417	52.9298	5.27718×10^{-32}	6.57574×10^{-6}
Blue	10^{-4}	-1	1.9245×10^{-5}	1.5	115	20	55.0234	55.3450	8.40563×10^{-35}	6.57969×10^{-6}
Black	10^{-4}	-1	1.9245×10^{-5}	1.5	120	20	57.5058	57.8274	1.87223×10^{-35}	6.58331×10^{-6}
Cyan	10^{-4}	-1	1.9245×10^{-5}	1.5	123	20	58.9956	59.3172	2.43366×10^{-33}	6.58534×10^{-6}

Table 11: Feasible parameter sets for inflation for $\rho = 3$. In these sets, $T'_{\text{Rhc}} = T'_{\text{Ihc}} = 10^{-5}M_{\text{pl}}$. N_{end} is the e-folding number when $\epsilon = 1$, which represents the end of inflation. N_{stop} means the e-folding number that we stop the numerical calculation.

Color	$ \mu /M_{\text{pl}}^2$	ν_1/M_{pl}	$T_{\text{Rend}}/M_{\text{pl}}$	$T_{\text{Rhc}}/M_{\text{pl}}$	$T_{\text{Ihc}}/M_{\text{pl}}$	$T'_{\text{Rhc}}/M_{\text{pl}}$	$T'_{\text{Ihc}}/M_{\text{pl}}$	N_{end}	N_{stop}	β_{iso}	$\cos(\Delta)$
Cyan	10^{-4}	-1	1.5	105	60	10^{-5}	10^{-3}	50.061	50.3826	9.20002×10^{-36}	3.28604×10^{-4}
Black	10^{-4}	-1	1.5	105	50	10^{-5}	10^{-2}	50.061	50.3826	1.82773×10^{-30}	3.2857×10^{-3}
Blue	10^{-4}	-1	1.5	105	40	10^{-5}	10^{-1}	50.061	50.3826	4.48765×10^{-39}	3.28483×10^{-2}
Green	10^{-4}	-1	1.5	105	30	10^{-5}	1	50.0607	50.3823	1.87863×10^{-9}	3.203×10^{-1}
Red	10^{-4}	-1	1.5	105	20	10^{-5}	2	50.0599	50.3815	6.73078×10^{-7}	5.7951×10^{-1}

Table 12: Parameter sets for showing the significant turning in $\rho = 3$ case. The difference of each parameter sets lie in $T'_{\text{Ihc}}/M_{\text{pl}}$, the initial rate of T_I and the initial coordinate of T_I . N_{end} is the e-folding number when $\epsilon = 1$, which represents the end of inflation. N_{stop} means the e-folding number that we stop the numerical calculation.